ENERGY RELEASE RATES IN DELAMINATION OF GLASS FABRIC REINFORCED COMPOSITE LAMINATES

by

M. D. NARAYANAN

DEPARTMENT OF MECHANICAL ENGINEERING

INDIAN INSTITUTE OF TECHNOLOGY, KANPUR

AUGUST, 1988

ENERGY RELEASE RATES IN DELAMINATION OF GLASS FABRIC REINFORCED COMPOSITE LAMINATES

A Thesis Submitted
In Partial Fulfilment of the Requirements
for the Degree of

MASTER OF TECHNOLOGY

by

M. D. NARAYANAN

to the

DEPARTMENT OF MECHANICAL ENGINEERING

INDIAN INSTITUTE OF TECHNOLOGY, KANPUR

AUGUST, 1988

ME-1988-M-NAR-ENE

CERTIFICATE

This is to certify that the thesis entitled 'Energy Release Rates in Delamination of Glass Fabric Reinforced Composite Laminates' by M.D. Narayanan is a record of work carried out under my supervision and has not been submitted elsewhere for a degree.

Prashant Kumar

August, 1988

Dr. Prashant Kumar
Professor
Dept. of Mechanical Engineering
Indian Institute of Technology
Kanpur-208016, India.

ACKNOWLEDGEMENTS

I express my deep sense of gratitude and appreciation to Professor Prashant Kumar, for his valuable guidance throughout the present work.

I am thankful to Mr. Rakesh and Mr. V. Murti for the help rendered in the experimental investigation.

Thanks to Mr. Swaran Singh, Dr. Badri Rai and Mr. D.K. Sarkar for their help.

Thanks to Mr. B.K. Jain for the cooperation rendered in the experimental work.

I am also thankful to C.M. Abraham for the excellent typing of the manuscript.

M. D. Narayanan

CONTENTS

LIST OF FIGURES

LIST OF TABLES

NOMENCLATURE

G	energy release rate
G_I	mode I interlaminar fracture toughness
G_{II}	mode II interlaminar fracture toughness
H	potential energy
U	elastic strain energy stored in the body
W	work supplied by the external forces
A	crack area
P	load on the fracture toughness testing specimen
P_c	critical load on the fracture toughness testing specimen
u	crack opening displacement or load point displacement
C	compliance of the specimen
G_{IC}	critical mode I interlaminar fracture toughness
G_{IIC}	critical mode II interlaminar fracture toughness
EI	fluxural rigidity
a	crack length in the specimen
w	width of the specimen
A_1, A_2	constants obtained from the log-log plots of DCB specimen
h	semi-thickness of the ENF specimen
L	half span in ENF testing
E	total energy of the impactor
E_d	energy dissipated in damage zone
E_{del}	energy dissipated in delamination

A_{del}	total delamination area of the impacted panels
f	fraction of energy of the impactor absorbed in the hanging plate
E_p	total energy absorbed in the hanging plate
u_c	critical displacement for DCB specimen

ABSTRACT

Interlaminar fracture toughness of glass fabric reinforced epoxy laminates has been investigated experimentally. Fracture toughness tests are conducted on double cantilever beam specimens to get G_{IC} and on end notched flexure specimens to get G_{IIC}. Various experimental data reduction methods for finding G_{IC} are examined and the compliance method is chosen as the best one.

Ballistic impact tests are conducted on laminates made of same material. The delamination occurred due to impact is measured using a destructive technique. The results of fracture toughness tests are applied to the impact to get the energy dissipated in delamination. Contrary to the expectation, the energy of impactor absorbed in delamination is found to be quite low.

CHAPTER 1

INTRODUCTION

1.1 INTRODUCTION

A composite is a combination of material created by assembly of two or more components - a selected filler or reinforcing agent and a compatible matrix binder. This can achieve a combination of properties not achievable by any of the component materials acting alone.

Laminated fibre composites are now increasingly used in structural members of aircrafts because they offer attractive properties such as light weight, high specific strength and stiffness.

There is growing demand for the composite material which can replace metals in many operating conditions (for example, in aircraft structures). This has led to the development of more sophisticated constituent materials and better design. One of the common problems in using laminates is that they are very susceptable to impact damage and aircraft structures have to be designed to sustain such damages. In comparison with the conventionally used metals, the laminates are less tough and fracture cracks caused by an impact spreads to longer distances. Since the damage can spread in the interfaces between the various plies which are not visible from outside, it may not be detected easily.

As a result of durability and damage tolerance considerations, impact and delamination resistance have become key issues when composite materials are used in structural applications [1].

1.2 MECHANISMS OF FAILURE

A great variety of deformation modes can lead to failure of the composite. The operative failure mode depends on the loading conditions and the microstructure of the composite, fibre diameter, volume fraction of fibres, fibre distribution etc. In the case of composite materials, internal material failure generally initiates much before any change in its macroscopic appearance or behaviour is observed [2]. The material failure may be observed in many modes such as (i) breaking of the fibres (ii) microcracking of the matrix (iii) separation of fibres from the matrix (called debonding) and (iv) delamination (separation of laminae from each other): These modes may act separately or jointly.

1.3 DELAMINATION - A MAJOR FAILURE MODE

As a result of the laminated nature of most composite structures, two principal transverse directions must be considered, which are perpendicular to one another, namely, the interlaminar and the translaminar directions. Correspondingly two different failure modes are considered with fracture propogating either between or across the layers of the laminate [3].

Due to the absence of through the thickness reinforcement, the laminate is prone to interlaminar failure or delamination.

Delamination has been observed as one of the most frequently encountered type of damage in composites. The presence and growth of delamination cracks result in the progressive reduction of stiffness and strength of composites. These lead to the loss of structural integrity and contribute to the final failure of the structure. Thus, understanding the behaviour of delamination crack growth (propagation) under different loading conditions is of fundamental importance.

Delamination takes the form of separation of plies under mechanical, thermal or environmental loading. Potential sites for initiating an interlaminar crack may include geometric discontinuities, processing and machining defects and manufacturing flaws. The delamination also occurs due to impact on a laminate. This problem is unique to composites and is not observed in metals and polymers in general. Since the material properties are discontinuous in the thickness direction due to the lamination process and since the interlaminar strength is generally very low in the interlaminar region, defects such as microcracks, voids, inclusions, broken plies etc. tend to grow in an interlaminar mode. It is also known that interlaminar fracture toughness is low compared to that parallel to the fibres [4]. Also, in the case of through the

thickness impact, delamination can be a major failure mode. In such a case delamination acts as perhaps the weakest link in the chain of failure process.

1.4 FRACTURE MECHANICS CONCEPTS

The early development of fibre composites for high performance was mainly concerned with achieving high modulus and high strength materials. But high strength is not sufficient as some of the materials developed are of a brittle nature with small elongation to fracture. One of the most important performance criteria should be the ability to absorb energy and resist impact loading [5].

The energy absorption or toughness of homogeneous isotropic materials has been measured by various techniques such as edge notched tension test, cleavage tests, charpy, izod and drop weight impact tests. The results obtained for brittle materials could often be correlated with fracture mechanics theories such as Griffith theory for fracture of brittle materials. However, when theories developed for single-phase materials are applied to fibre composites the behaviour cannot be easily predicted. The fracturing process for composites is much different from homogeneous materials and the energy absorption can certainly not be calculated by application of the 'rule of mixtures' to the two or more phases.

The interlaminar failure occurs mostly by either one of two modes designated Mode I and Mode II. In the first, failure is produced by a stress applied at right angle to the laminate plane, resulting in opening up of the laminate (opening mode), and in the second, failure is caused by an in-plane shear stress (forward shear mode). Another less common failure is in anti-plane shear stress (parallel shear mode).Often a combination of stresses produces a mixed-mode failure. The above three modes of failures are shown in Fig. 1.1.

1.5 ENERGY RELEASE RATE 'G'

The equilibrium of an existing crack may be judged from the intensity of elastic stress around the crack tip or by energy release rate G.

Associated with various modes, stress intensity factor can be defined. But the stress analysis ahead of the crack tip in a composite material is an extremely difficult problem because of the local heterogenity and anisotropy. Thus, it has become a common practice to characterise interlaminar fracture with the strain energy release rate G. This quantity is based on energy considerations and is mathematically well defined as well as physically measurable in experiments.

In the application of the energy principle it is not necessary to specify the constitutive properties of the system. Also the body may be isotropic or anisotropic, elastic or

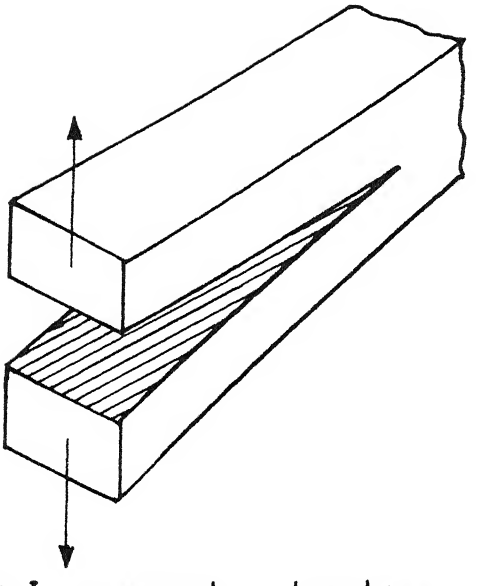

(a) Mode I symmetric loading
(opening mode)

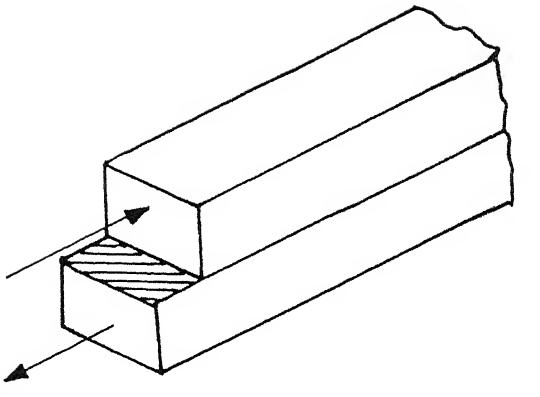

(b) Mode II · skew symmetric
shear loading
(forward shear mode)

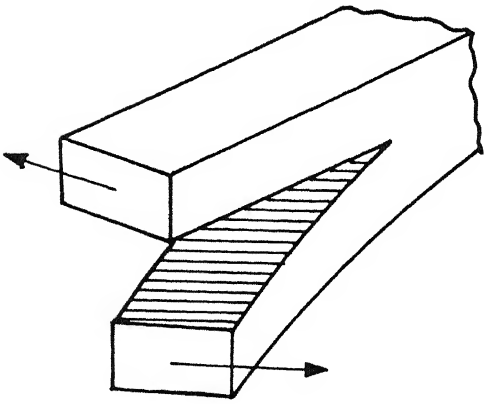

(c) Mode III · antiplane shear loading
(parallel shear mode)

Fig.1.1 Modes of crack surface displacement.

inelastic, linear or nonlinear.

1.6 DETERMINATION OF ENERGY RELEASE RATE 'G'

Interlaminar fracture toughness is determined by suitable methods. Out of the three modes of interlaminar failure mentioned earlier, the mode I fracture toughness determination is well established. The mode II, fracture toughness determination is not so much investigated. For Mode III fracture toughness standard test methods are not so far available because of the difficulty to get a pure mode III failure.

In the literature, there are a number of reports concerned with the measurement of mode I interlaminar fracture toughness in composite materials. The double cantilever beam (DCB) type configuration is one of the most common specimen geometries.

Paul E. Keary et al. [6] have used double cantilever beam specimen to measure interlaminar fracture toughness in mode I. They analysed the data through several different schemes and compared them with one another. For characterising the behaviour of delamination and fracture analysis for separation of modes, D.J. Wilkins et al. [7] have found critical strain-energy release rate for mode I and mode II delamination. They have used DCB specimen for mode I fracture study and cracked lap shear (CLS) specimen that for mode II. Han and Koutsky [8] have found interlaminar fracture energy of glass fibre reinforce

polyster composites using width tapered double cantilever beam (WTDCB) specimens. Devitt, Schapery and Bradley [9] developed a nonlinear theory for energy release rate using DCB.

D. Guedva et al [10] have made a comparitive study of various test methods for fracture toughness in Mode I using DCB specimens. In order to study the various steps in the delamination failure in mode I Charentenay and Benzeggagh [11] have used DCB to get accoustic emission signals in the crack propagation process. They identified three distinct stages of crack propagation.

DCB specimen was used in the investigation of loading rate effect on interlaminar fracture toughness by Mall, Law and Katouzian [12] and Smiley and Pipes [13].

For mode II interlaminar fracture toughness determination only a few references are available mainly because no standard specimen is available for individual characterization of this mode. Carlsson et al [14] has used end notched flexure (ENF) specimen for finding Mode II fracture toughness. They also analysed the effect of shear deformation and the influence of friction between the crack surfaces in the fracture toughness evaluation. The ENF specimen has been used by G. Moron et al [3] to determine mode II interlaminar fracture toughness for various types of fibre reinforcement.

1.7 IMPACT BEHAVIOUR OF COMPOSITE LAMINATES

Impact response is an essential parameter for determining the suitability of a composite material for high strain-rate applications. Although the response of composite materials and structures to static load is well established, no comparable studies are available for response of composite laminates against foreign-impact object. One of the most important difficulties for applying these materials to impact conditions, is the great deal of variable which influence on absorbed energy. In composites with one reinforcing phase, the impact response is a function of material parameters such as orientation, volume fraction and constituent properties and of testing parameters such as impact energy and speed, size and shape of the impactor, support conditions of the target, the direction of impact etc.

Many investigators have studied the damage caused by the projectile on fibre composite laminates. The main emphasis had been to find the relation between the total damage area and projectile velocity (or impact energy). Most of the work has been experimental.

Graham Dorey [15] has reviewed the properties particular to advanced composites emphasizing the failure mode and energy absorbing mechanisms. The damage produced under impact loading and its effect on residual mechanical performance are explained.

Sierakowski and Chaturvedi [16] in their article summarise various works on impact loading response of filamentary type composite materials.

The influence of various material and testing parameters on impact behaviour of composite laminates was studied by Liceaga and Imaz San Miguel [17].

1.8 OUTLINE OF THE PRESENT WORK

In the present work specimens with artificial cracks were prepared in the laboratory. Fine woven glass cloth reinforcement was used in sixteen layers with epoxy resin as the matrix to get composite plate of thickness about 3 mm.

To find the mode I interlaminar fracture toughness (G_I) double cantilever beam (DCB) specimen was prepared and was tested in tensile mode.

For Mode II interlaminar fracture toughness (G_{II}) determination, end notched flexure (ENF) specimen was used. The specimen was tested in three point bending.

Ballistic impact experiment was conducted on the composite laminates. The target plate was clamped and impacted by a projectile accelerated in an air gun.

It is expected that considerable amount of incident energy gets dissipated in forming delamination cracks. In this study

attempt is made to get the fraction of energy absorbed in delamination caused by impact. With this study it is expected to know the role of delamination in the total failure process.

Using a destructive method the delamination area of the impacted laminate was measured. The results obtained by the fracture toughness tests were used to find the energy absorbed in delamination due to impact.

In Chapter 2 the details of finding the mode I interlaminar fracture toughness with the experimental method are presented. Several experimental data reduction methods are examined. In Chapter 3 the theoretical and experimental aspects of mode II interlaminar fracture toughness determination are explained. The details of impact test on composite laminates are given in Chapter 4. The results of the work and discussion are given in Chapter 5. Chapter 6 concludes the present work.

CHAPTER 2

MODE I INTERLAMINAR FRACTURE TOUGHNESS DETERMINA

2.1 INTRODUCTION

Delamination or interlaminar failure is a common failure mode observed in composite material. In this chapter the experimental method for determining the mode I fracture toughness in delamination is explained with the necessary theory. Energy release rate 'G' is chosen as the suitable parameter to characterise fracture toughness. A double cantilever beam (DCB) specimen is used for the test. Different methods of experimental data analysis are explained.

2.2 EXPRESSION FOR ENERGY RELEASE RATE 'G'

It has become a common practice to characterise interlaminar fracture toughness with strain energy release rate 'G'. The energy approach is based on a thermodynamic criterion for fracture by considering the energy available for crack growth of the system on one hand and the surface energy required to extend an existing crack on the other hand. A potential energy H may be defined for a cracked body as

$$H = U - W \qquad (2.1)$$

where U is the elastic strain energy stored in the body and W is the work supplied by the movement of the external forces.

If G_c is the work required to create a unit crack area, the criterion for crack growth can be written as

$$\delta H \geq G_c \ \delta A$$

where δA is the increase in crack area.

For critical conditions the equality sign and for unstable crack growth inequality sign holds good.

The strain energy release rate, G is defined as

$$G = - \frac{\partial H}{\partial A} \qquad (2.2)$$

in terms of G, the fracture criterion may be formulated as

$$G \geq G_c$$

This concept will be illustrated for a linear elastic body containing a crack of length a and a $+\Delta$ a respectively. Fig. 2.1 shows the load P versus displacement u behaviour for the cracked body where crack growth is assumed to occur either at constant load (fixed load) or at constant displacement (fixed grip).

For fixed load case, referring to Fig. 2.1 we have,

$$\delta U = \text{Area ADE} - \text{Area ABC}$$

$$= \frac{1}{2} P(u + \Delta u) - \frac{1}{2} pu$$

$$= \frac{1}{2} P \Delta u$$

$$\delta W = P \Delta u$$

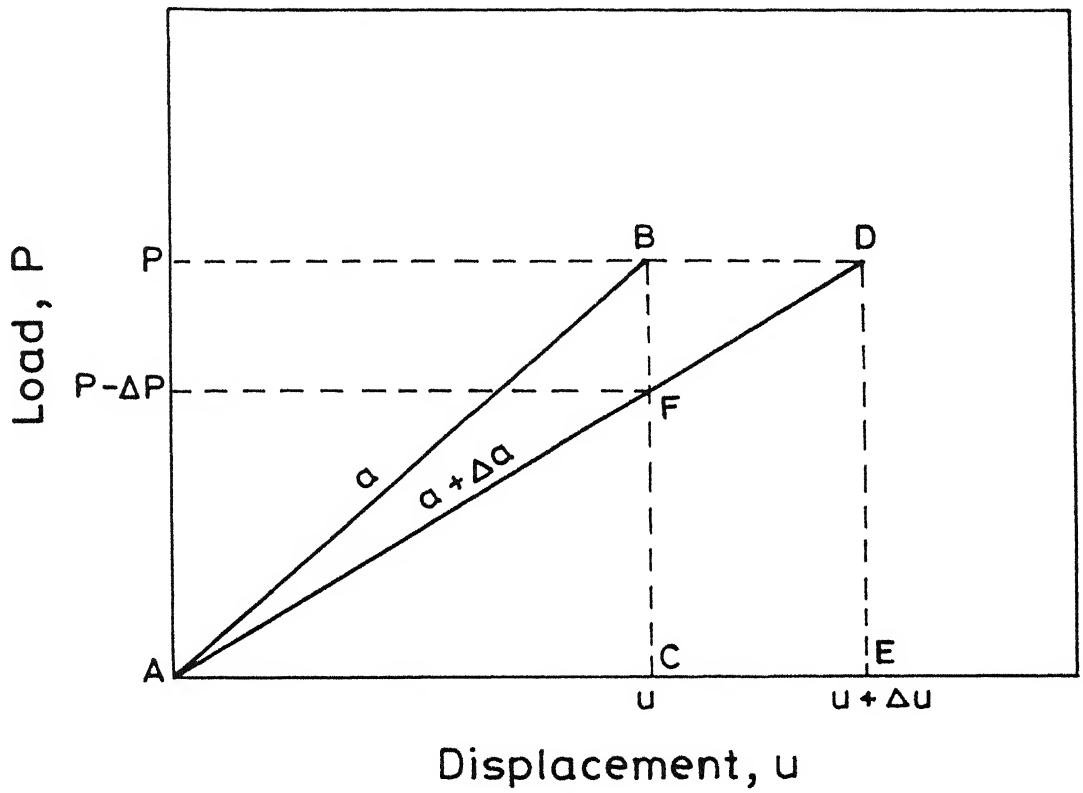

Fig. 2.1 Load-displacement behaviour for a cracked body.

Eq. (2.1) gives

$$\delta H = \frac{1}{2} P \Delta u - P \Delta u = - \frac{P \Delta u}{2}$$

and Eq. (2.2) gives

$$G = \frac{P}{2} \frac{\partial u}{\partial A} \qquad (2.3)$$

For fixed grip case, the work term vanishes and from Fig. 2.1 we have,

$$\begin{aligned} \delta U &= \text{Area AFC} - \text{Area ABC} \\ &= 1/2\ (P + \Delta P)u - 1/2\ Pu \\ &= \frac{u \Delta P}{2} \end{aligned}$$

and $$G = - \frac{u}{2} \frac{\partial P}{\partial A} \qquad (2.4)$$

For a linear elastic body, the relation between the load and displacement may be expressed as

$$u = CP$$

where C is the compliance of the specimen.

Substitution of this into Eq. (2.3) (fixed load) gives

$$G = \frac{P^2}{2} \frac{\partial C}{\partial A} \qquad (2.6)$$

and substitution of P = u/C into Eq. (2.4) (fixed grip) gives

$$G = \frac{u^2}{2C^2} \frac{\partial C}{\partial A} = \frac{P^2}{2} \frac{\partial C}{\partial A} \qquad (2.7)$$

Consequently both Eqs. (2.3) and (2.4) reduce to the same expression. This expression will be used for experimental determination of G.

2.3 DOUBLE CANTILEVER BEAM (DCB) SPECIMEN

Double cantilever beam specimen (Fig. 2.2) is the most commonly used specimen [7,10] for measuring mode I delamination fracture toughness. Other geometries such as width tapered double cantilever beam [4,8] are not as popular as straight sided specimen.

Analysis of DCB specimen

The test specimen was initially developed for investigation of adhesive fracture mechanics. Because of the similarity between the debonding process in metals and the delamination process in composites, DCB specimens were utilized for composites.

Our approach is based on concepts of linear-elastic fracture mechanics carried out for isotropic materials. Various geometric and material properties lead us to assume that these concepts could be applied successfully [18] :

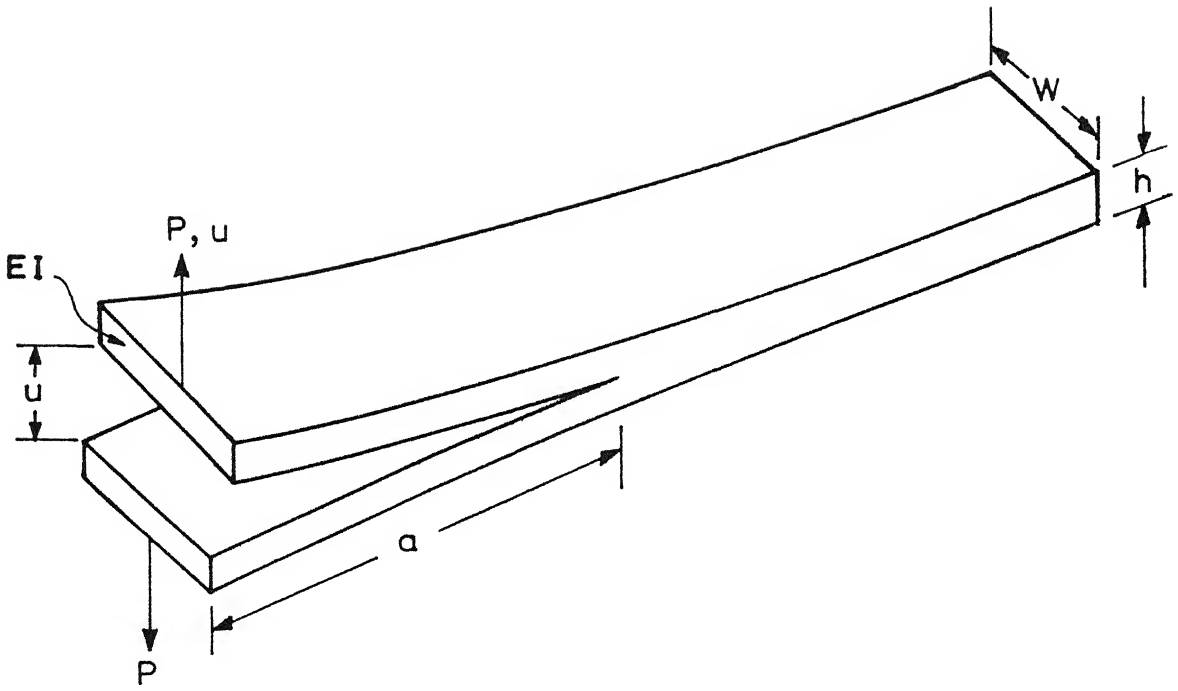

Fig. 2.2 Double cantilever beam specimen.

Firstly the interlaminar crack is essentially planar and the crack tip is evenly distributed across the width of the specimen. Secondly the crack plane is normal to the loading axis. Thirdly, the beam behaves elastically at the macroscopic scale.

The compliance of the DCB specimen (Fig. 2.2) $C(=u/P)$ may be obtained from elastic beam theory as [19]

$$C = 2a^3/3EI \tag{2.8}$$

where a is the crack length and EI is the fluxural rigidity of each beam of the specimen. The factor 2 appears because of the double cantilever.

$$G_I = \frac{P^2}{2}\frac{\partial C}{\partial A} = \frac{P^2}{2w}\frac{\partial C}{\partial a} \tag{2.9}$$

where P is the applied load and w is the width of the specimen. From Eqs. (2.9) and (2.8) we have,

$$G_I = P^2a^2/wEI$$

Critical conditions occur when G_I reaches its critical value G_{IC} for the critical load $P = P_c$

$$\text{Thus,} \quad G_{IC} = \frac{P_c^2\, a^2}{wEI} \tag{2.10}$$

2.4 STABILITY OF CRACK GROWTH

Stable crack growth requires dG/da to be less than or equal to zero

$$dG/da \leq 0$$

For DCB specimen under fixed load condition using Eq. (2.3) and Eq. (2.8) we get,

$$\frac{dG_I}{da} = \frac{2P^2a}{wEI} \tag{2.11}$$

Since this quantity is always positive the crack growth is unstable.

For fixed grip condition, substitution of P = u/C and Eq. (2.8) in Eq. (2.4) gives

$$\frac{dG_I}{da} = -\frac{9u^2EI}{wa^5} \tag{2.12}$$

where u is the displacement of grips.
This quantity is always negative and thus the crack growth is stable. Experimentally most testing is performed under fixed grip conditions (displacement control) which render the crack growth stable.

The fact that the crack growth is stable under controlled displacement test can be further explained with the help of strain energy versus crack length diagram shown in Fig. 2.3 [6]. It is clear that increasing the load or grip displacement for a fixed crack length will increase the strain energy stored.

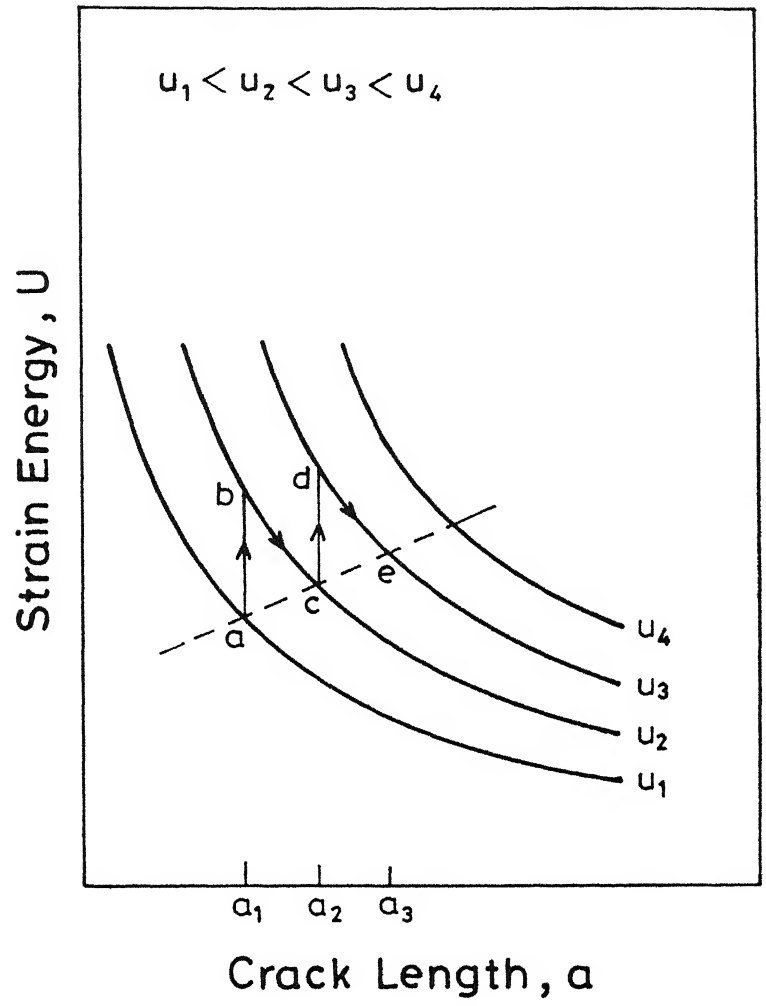

Fig. 2.3 Schamatic diagram of strain energy versus crack length for constant grip displacement.

Also it is apparent that crack extension which occurs at constant grip displacement results in a decrease in strain energy stored in the specimen as shown in Fig. 2.3. As the specimen with fixed crack size a_1 is deformed from u_1 to u_2, the strain energy obviously increases. The strain energy release rate also increases as the test goes from a to b. Suppose at b the critical energy release rate is exceeded slightly and crack extension for constant u occurs, changing the crack length from a_1 to a_2. At point c the energy release rate is again insufficient to give crack extension, so that further loading to point d is necessary, which again corresponds to G being slightly larger than the critical energy release rate, G_c. Crack extension occurs from a_2 to a_3 as one moves along d-e. We may conclude from these considerations that crack growth is stable in a controlled displacement test if G_c does not change with crack length (or at least, if it does not decrease rapidly with crack length).

In an actual test the loading and crack extension occur more or less continuously, instead of in steps. Indeed with negligible kinetic energy (quasi-static loading and slow crack growth) the energy release rate is essentially equal to G_c at all times. The path a-c-e for $G = G_c$ represented by the dotted line (not necessarily straight) in the figure would be followed in an actual experiment.

2.5 FABRICATION OF DCB SPECIMEN

The DCB specimen was made in the laboratory through a hand lay up casting procedure. The details of the casting procedure for a composite plate is provided in Section 4.2.

DCB Specimen Geometry

Material - Glass fabric reinforced plastic

Length L = 22 cm

Initial crack length $a_o \cong 4$ cm

Width w = 2.54 cm

Thickness h $\cong$ 3 mm

Fabrication Details

A thin (0.025 mm thickness) aluminium coated mylar sheet was used to create an artificial crack in the laminates during the casting stage. The sheet was folded and kept at one end in the midplane while fabricating the plate as shown in Fig. 2.4a. The open end of the folded sheet was on the outer side of the plate. The size of the crack starter in the casting was adjusted to have more than the required initial crack length. The rest of the fabrication process of the plate is as described in Section 4.2.

The specimens of the above mentioned size (Fig. 2.4b) were cut from the plate. The sides were smoothened by rubbing on sand paper of different grades. For applying tensile load in tearing mode, two metallic hinges (load tabs)

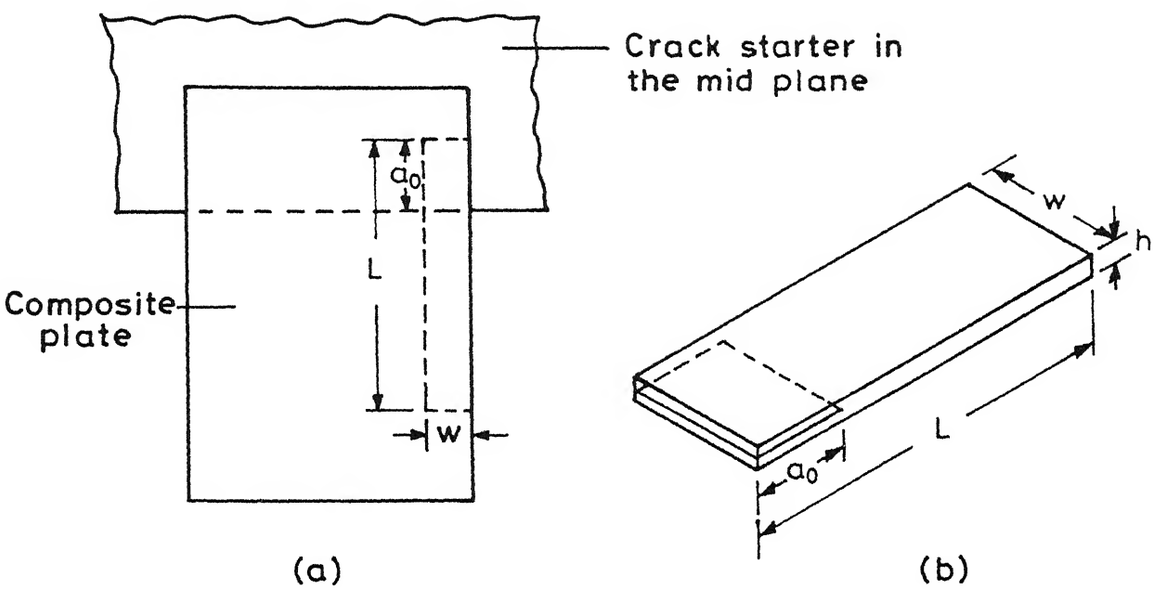

L = 220 mm
a_0 = 75 mm
w = 25.4 mm
h ≃ 3 mm

Fig. 2.4 Preparation of DCB specimen.

were attached on both sides of the specimen on the crack side as shown in Fig. 2.5. Aluminium hinges were selected for the purpose. For bonding the hinges properly to the specimen the following procedure was adopted.

Hinge Preparation : The bonding surface of the hinges were roughened by punch marks and saw cuts. The surfaces were cleaned by soap and after drying they were soacked in acetone. Afterwards the surfaces were not touched by hand.

Composite Surface Preparation : The surface was rubbed with coarse sand paper in $\pm$ 45^{o} directions. Also saw cuts were made on the surface in the same directions. The surface was washed with soap and water and after drying it was cleaned with acetone.

The hinges were attached to the specimen through araldite adhesive available in the tube form. Care was taken not to get any adhesive in the hinges, which will influence the moment free rotation aimed for. The hinges were aligned properly by using a mounting jig. The details of jig is given in Appendix A. After the adhesive was applied the hinges were clamped until the adhesive was cured. Care was taken not to misalign the hinges when the clamping pressure was applied.

After removing from the clamp, the specimen sides were coated with white typewriter correction fluid for making the

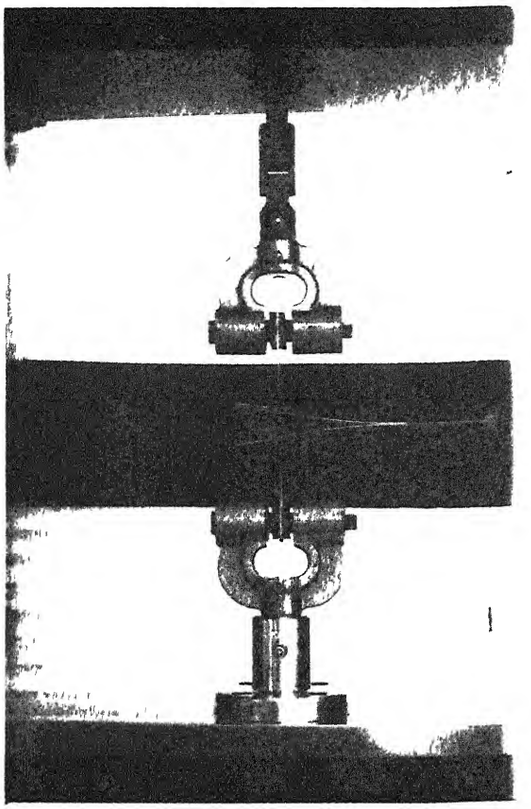

Fig. 3.3 DCB specimen with the loading hinges

crack propogation visible. Reference marks were made at equal intervals (about 8 mm) along the length on the wide surface of the specimen as an aid in testing.

2.6 EXPERIMENTAL DETAILS

The specimen was mounted on a properly aligned and calibrated Instron machine. Using two light springs attached at the free end of the specimen, it was kept always horizontal during the test (Fig. 2.6). The specimen was tested in tensile mode in the displacement control. A crosshead speed of 5 mm/min was used. The load cell used was 10 kN (maximum capacity) and the load range set was 0.05 kN. A real time display of load versus deflection was obtained. When the crack extended about 8 mm (to the marking on the specimen) the machine was stopped and time was given for crack to self arrest. (The crack propogation could be seen from the load-deflection curve as a sudden change in the slope of the curve in the beginning, followed by irregular ups and downs. Also the audible sound made the crack advance apparent). Then the crack tip position was marked with the aid of a magnifying lens on both sides of the specimen. And the specimen was unloaded and the machine was stopped at zero load. The specimen was loaded again to get similar kind of loading-unloading curve for the new crack

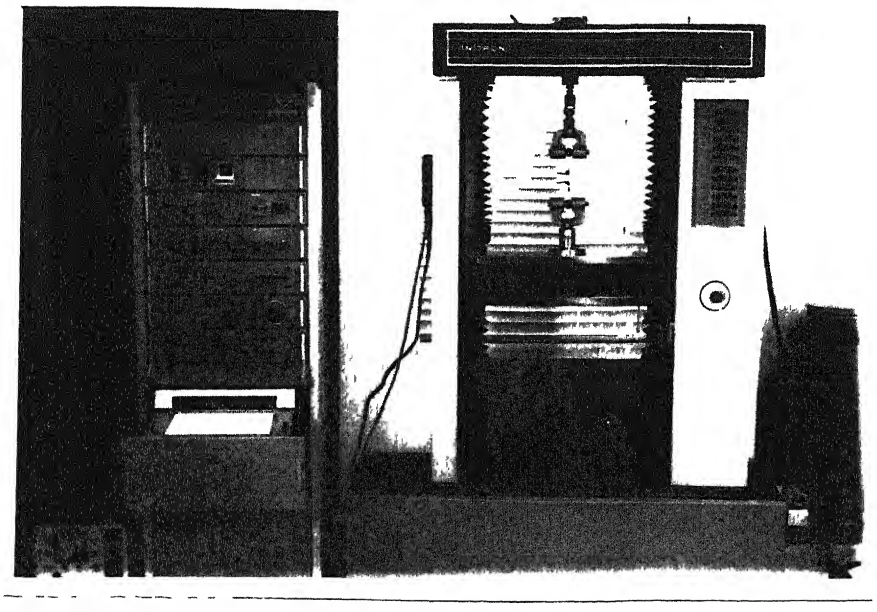

Fig. 2.6 DCB specimen loading set-up

length. About 5-7 cycles were conducted, each time marking the crack position after crack arrest. A typical load-displacement plot of the test is shown in Fig. 2.7. a_o, a_1 and a_2 are the crack lengths for successive loadings. Critical loads for the crack propogation are P_{co}, P_{c1} and P_{c2} and corresponding critical crack opening displacements are u_o, u_1 and u_2.

2.7 METHODS OF DETERMINING G

The measurement of fracture toughness for a material relies heavily on the method of data interpretation. In its raw form, static fracture data normally consists of a load-displacement record for specimens with cracks. Reduction of the data requires knowledge of the specimen (e.g., crack length and specimen dimensions) and theoretically based approach to calculate the fracture parameters.

Different schemes are available such as

1) Compliance method
2) Area method
3) Modified area method
4) Method using analytical formula
5) Method using nonlinear beam theory

i) Compliance calibration of linear elastic strain energy release rate

The crack length for each loading (Fig. 2.7) were

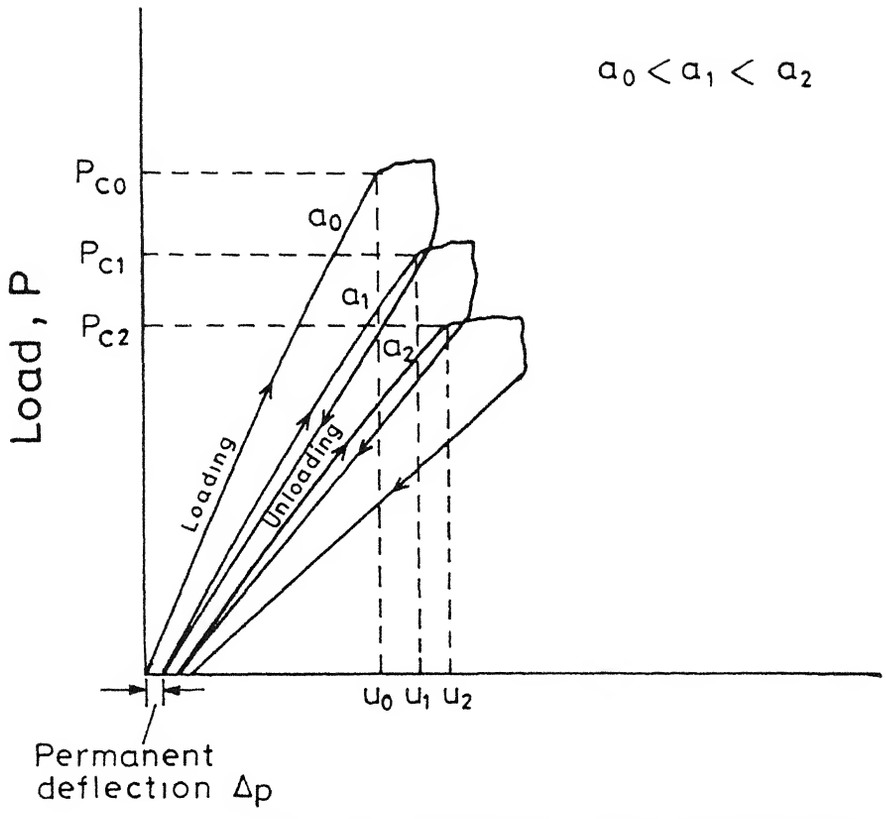

Fig. 2.7 A schematic load displacement diagram of DCB Mode I test.

measured as a_o, a_1, ..., a_n. The distance from the loading line to the crack marking along the specimen was taken as the crack length. The critical load for crack initiation for each crack length was obtained from the graph as P_{co}, P_{c1}, ..., P_{cn}. The compliance of the specimen C_o, C_1, ..., C_n for each crack length was calculated from C = u/P from each loading curve [7,20].

We have

$$C = 2a^3/3EI \tag{2.13}$$

and $$G_{IC} = P_c^2 a^2/wEI \tag{2.14}$$

Eq. (2.13) can be written as

$$C = A_1 a^3 \tag{2.15}$$

where $A_1 = 2/3EI$

Similarly, from Eq. (2.14)

$$P_c^2 = G_{IC}\, wEI\, a^{-2}$$

Or, $$P_c = \sqrt{G_{IC} wEI}\; a^{-1}$$

This can be written as

$$P_c = A_2 a^{-1} \tag{2.16}$$

where $A_2 = \sqrt{G_{IC}\, wEI}$

It can be seen that

$$G_{IC} = 3A_1 A_2^2/2w \tag{2.17}$$

A_1 and A_2 can be evaluated from the experimental data and using Eq. (2.17) G_{IC} can be evaluated.

To evaluate A_1 and A_2 experimentally, take logarithamic of Eq. (2.15) to obtain

$$\log C = \log A_1 + 3 \log a \qquad (2.18)$$

Experimental points of log C and log a are plotted on a graph and a straight line is fitted to the data with a slope equal to 3 by linear regression analysis or by hand. The line is extrapolated to crack length a = 1 mm. The compliance corresponding to a = 1 mm is A_1.

Similarly, from Eq. (2.16),

$$\log P_c = \log A_2 - \log a \qquad (2.19)$$

Points for log P_c and log a are plotted. A line is fitted with a slope equal to -1; the critical load value corresponding to a = 1 mm is A_2.

Knowing A_1 and A_2 and using Eq. (2.17) we obtain G_{IC} for the specimen.

This method of finding G_{IC} determination is most commonly used. The straight line fitting and the calculations can be done either manually or using a computer programme. A computer programme (Appendix D) was used for the purpose.

All the required data (such as critical load P_c) for the programme were taken from the P-u curve of DCB test. The straight line fittings between log-log values were done by the method of least squares.

ii) Area method

This method is a direct way to evaluate G_{IC}. The critical strain energy release rate may be determined from a loading-unloading sequence according to Fig. 2.8. From the definition of the strain energy release rate G_{IC} may be obtained as

$$G_{IC} = \frac{A}{w(a_2-a_1)} \qquad (2.20)$$

where A is the shaded area indicated in Fig. 2.8 and a_2-a_1 is the increment in crack length. The average of all the G_{IC} values for the entire range of loading-unloading gives the G_{IC} of the specimen.

In the present work the areas were found using a planimeter and G_{IC} was obtained directly using Eq. (2.20).

iii) Modified area method

Paul E. Keary et al. [6] argue that to interpret the actual area of the area method as the actual fracture energy is wrong. This can be explained as follows.

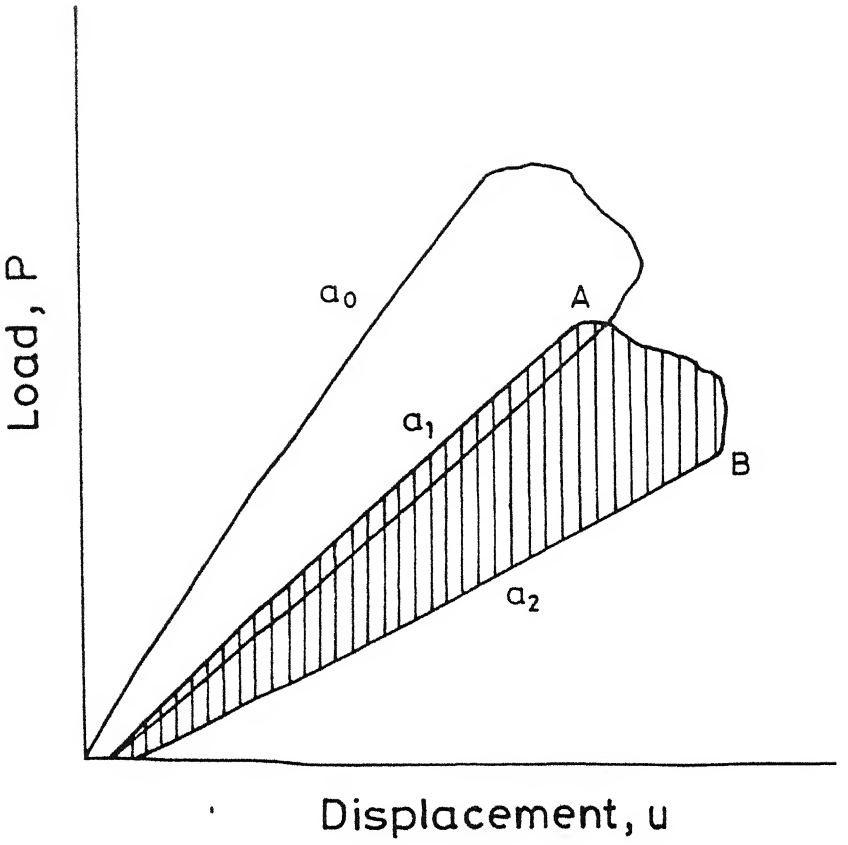

Fig. 2.8 Area method to evaluate G_{IC}.

Consider the arbitrary fracture specimen of Fig. 2.9a. The load versus displacement (P-u) response of the specimen is in general governed by a nonlinear elastic-plastic material behaviour at the tip of the crack. Fig. 2.9b shows the typical P-u curve for the specimen with crack length'a' until the point of crack extension. The total area under the curve is the work done in loading the specimen to the on-set crack extension. Unloading the specimen returns the linear and nonlinear components of elastic energy that are associated with a new crack length (a+da) as shown in Fig. 2.9c. When the specimen has been unloaded to zero load the remaining displacement is the permanent deformation Δp. Interpretation of the critical energy as the shaded region of Fig. 2.9c is wrong.

Fig. 2.9d shows a graphical representation of critical failure energy. The upper curve is equivalent to that of Fig. 2.9b. The lower curve shows the P-u curve of a similar specimen with a crack length a+da. The curve was drawn upto the displacement which is equal to the'u'associated with crack extension of the upper curve. The critical failure energy is the difference between the areas under the two curves shown by shaded region in Fig. 2.9d.

Thus a modification can be made by bringing all the loading curves of Fig. 2.8 to a common origin and finding the areas enclosed between them. Now the G_{IC} can be found using

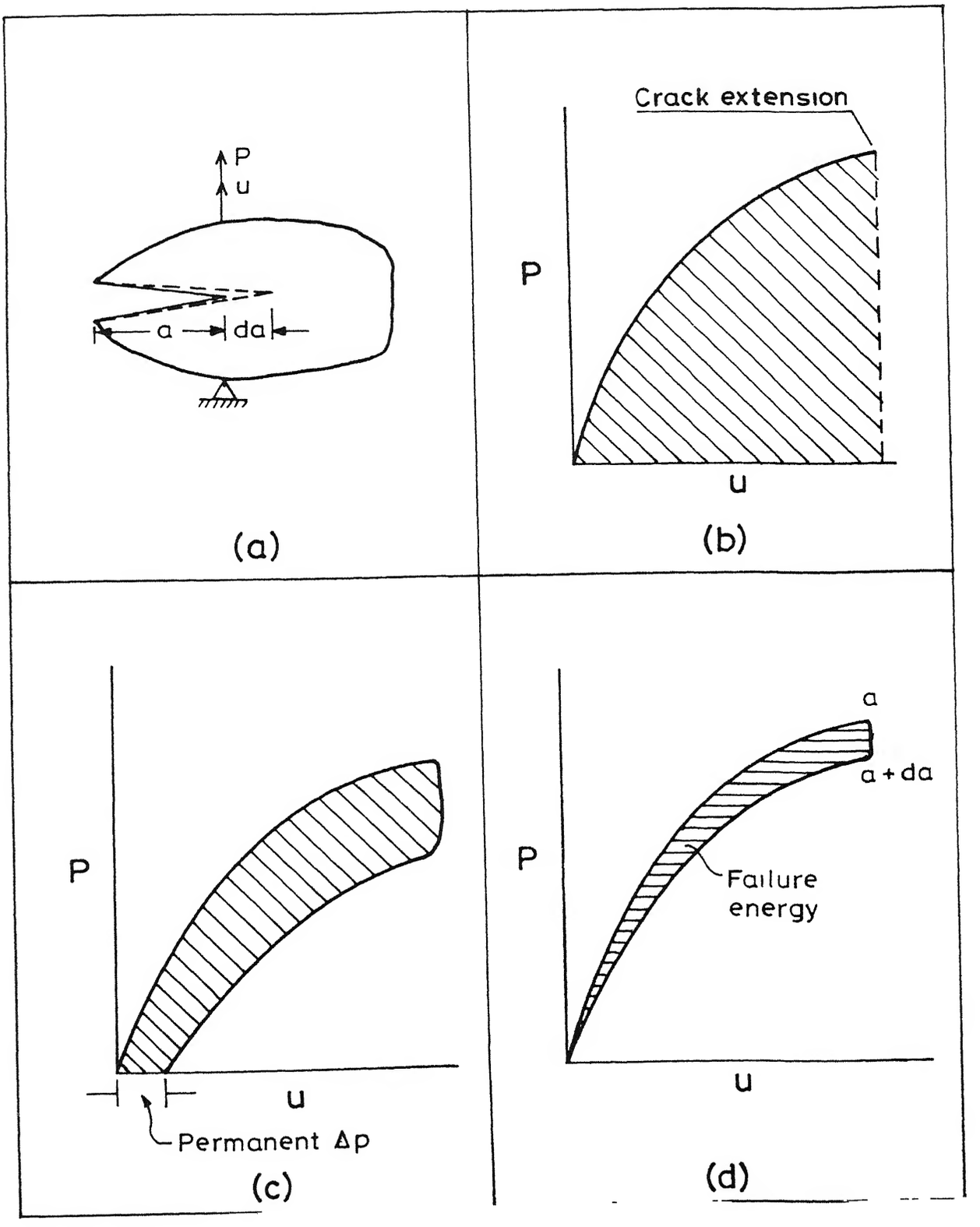

Fig. 2.9 The concept of failure energy.

the same formula as given in the Area method.

iv) Using formula

A simple way to find the energy release rate value from the test diagram would be to use a formula.

As shown in Sec. 2.3 compliance C and energy release rate G_I are given by

$$C = 2a^3/3EI \qquad (2.21)$$

and

$$G_I = P^2a^2/wEI \qquad (2.22)$$

Eq. (2.21) also gives

$$EI = 2a^3/3C$$

which is simplified further by substituting C = u/P in the above equation to get

$$EI = \frac{2a^3}{3(u/P)}$$

Using this equation, G_I of Eq. (2.22) is expressed as

$$G_I = \frac{3Pu}{2wa} \qquad (2.23)$$

G_{IC} values for $P = P_c$ for various crack lengths can be found and the average value will give the G_{IC} of the specimen.

v) Using nonlinear beam theory

As a result of low fluxural rigidity of thin composite specimen, large deflection and rotation may be present during the test. In order to avoid nonlinear (large) deflections, Paul E. Keary et al [6] in their work prescribed limits so that the data from all tests were performed to satisfy the inequality

$$u/2a < 0.2$$

where u is the load point displacement and a is the corresponding crack length.

In the present work thin composite plates of 3 mm thickness were chosen to make specimens because in actual applications sheets of about 3 mm thickness are generally used. Therefore, the beams were thin and slender and the above inequality could not be always satisfied. The apparent large deflections (especially at larger crack lengths) of the specimen, need to be accounted for in the analysis.

Incorporating the correction to linear beam theory, Devitt et al [9] has extended it to find the strain energy release rate for nonlinear deflections assuming linear stress-strain equations and small strains. The nonlinear beam variable obtained by them are given in the form of a table. In the present work their tables, relating u/a with Gw/2P were used.

The actual value of u/a corresponding to the critical loads (P_c) were found from the experiments on the DCB specimen. The corresponding $Gw/2P_c$ values were found from the table by linear interpolation.Knowing P_c and $Gw/2P_c$, G_c is calculated. The average of all the cycles was taken as the G_c value of the specimen.

CHAPTER 3

MODE II FRACTURE TOUGHNESS TESTING

3.1 INTRODUCTION

Delamination can occur by mode II failure. In this chapter the testing method for evaluation of energy release rate G_{II} is explained. End notched flexure (ENF) specimen is used for the experiment. The stability criterion for crack is also given at the end.

3.2 END NOTCHED FLEXURE TEST PRINCIPLE

The end notched flexure (ENF) specimen is shown in Fig. 3.1. The ENF fracture specimen is essentially a three point flexure specimen with an embedded through width delamination placed at the laminate midsurface. The purpose of the specimen is to determine the critical strain energy release rate in pure Mode II loading. It is shown in [14], that the specimen has been found to produce shear loading at the crack tip without excessive friction between the crack surfaces.

From elastic beam theory an expression for strain energy release rate can be derived [14,19] as

$$G_{II} = \frac{9P^2Ca^2}{2w(2L^3+3a^3)} \qquad (3.1)$$

where P is the applied load, C is the compliance, a is the crack length, w is the width of the specimen and L is the span between the central loading pin and the outer support pins. The derivation of the above equation is given in Appendix B.

The compliance of the beam may be calculated from the following formula based on beam theory [14,19]

$$C = \frac{2L^3 + 3a^3}{8Ewh^3} \tag{3.2}$$

where E is the flexural modulus in the axial direction of the beam and h is the semithickness of the beam. The compliance was determined experimentally rather than using the above formula. In the above derivations deformations due to the action of shear stress and influence of friction between the crack surfaces were neglected.

3.3 STABILITY OF CRACK GROWTH

The stability of crack growth can be determined from the sign of dG_{II}/da similar to as shown for DCB specimens in Sec.2.3.

For fixed load conditions Eqs. (3.1) and (3.2) give

$$\frac{dG_{II}}{da} = \frac{9aP^2}{8Ew^2h^3} \tag{3.3}$$

This quantity is always positive and hence crack growth is unstable.

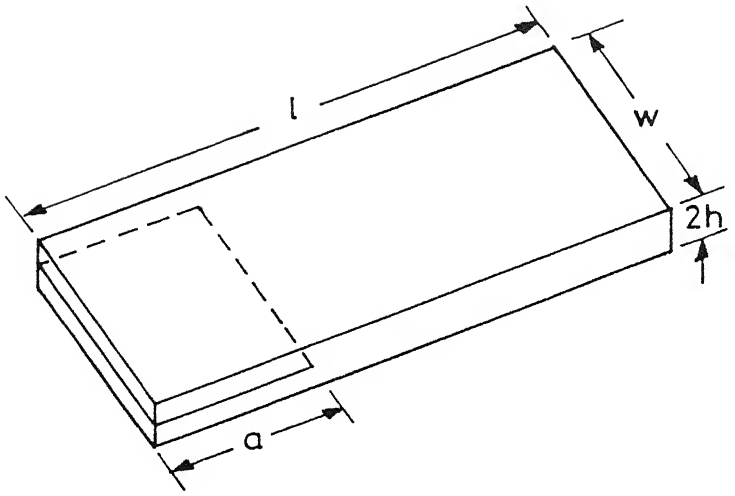

l = 112 mm
w = 26.5 mm
2h = ≃ 3 mm
a ≅ 30 mm

Fig. 3.1(a) Geometry of the ENF specimen.

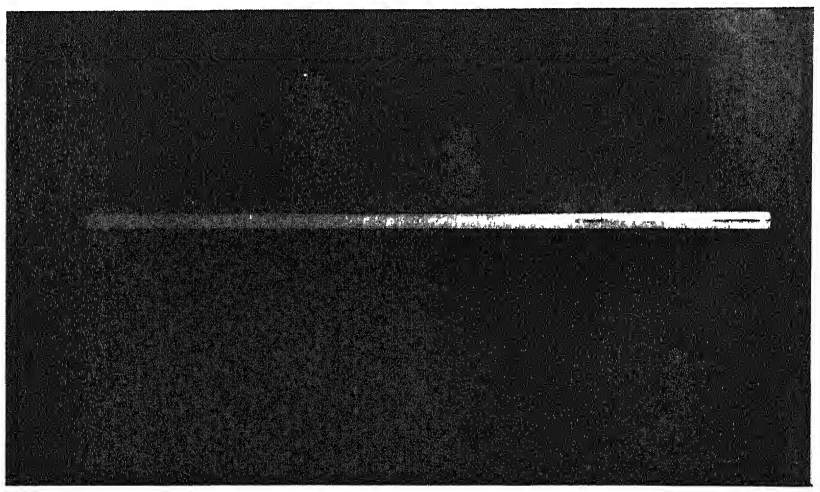

Fig. 3.1(b) Side view of the ENF specimen.

For fixed grip conditions, substituting P = u/C (where u is the centre load point displacement) in Eq. (3.1) and using Eq. (3.2) we get,

$$\frac{dG_{II}}{da} = \frac{9u^2a}{8Ew^2h^3C}\left[1 - \frac{9a^3}{(2L^3+3a^3)}\right] \qquad (3.4)$$

For stable crack growth $\frac{dG_{II}}{da}$ has to be less than or equal to zero. This gives

$$a \geq L/3^{1/3} = 0.7\ L$$

Since in the present testing $a \leq L/2$ the crack growth is unstable even under fixed grip conditions.

From the load displacement curves of the ENF test the compliance C and the critical load P for crack propagation are determined and G_{IIC} is computed using Eq. (3.1).

3.4 PREPARATION OF ENF SPECIMEN

The ENF specimen is as shown in Fig. 3.1. Both the ENF and DCB specimens were cut from the same plate. The method of fabrication of DCB specimen as explained in Sec. 2.4 is followed for the fabrication of ENF specimen. The sides of the specimen were smoothened by sand paper. The dimensions chosen were slightly different from those given in Carlsson and Pipes [20]. The minor changes in dimensions were necessary to accommodate the specimen in the available loading fixture in the testing laboratory.

3.5 EXPERIMENTAL DETAILS

The specimen was subjected to three point bending on a properly aligned and calibrated Instron machine. The specimen loading test set-up is shown in Fig. 3.2. The test was carried on in displacement control. A cross head speed of 1 mm/min was used. The load cell was 100 kN (maximum capacity) and the load range set was 1 kN. A real time plot of the load versus displacement was made on an x-y recorder. Only one loading cycle can be performed for each specimen since the crack growth is unstable.

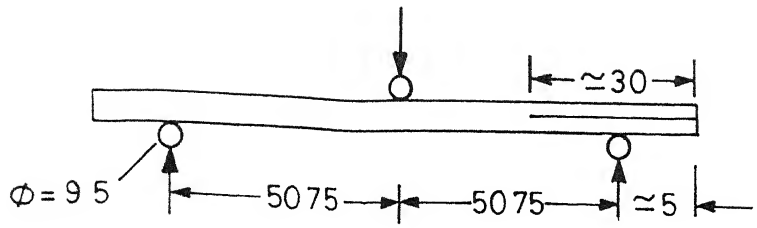

(All dimensions are in mm)

Fig. 3.2(a) ENF loading of the specimen in mode II.

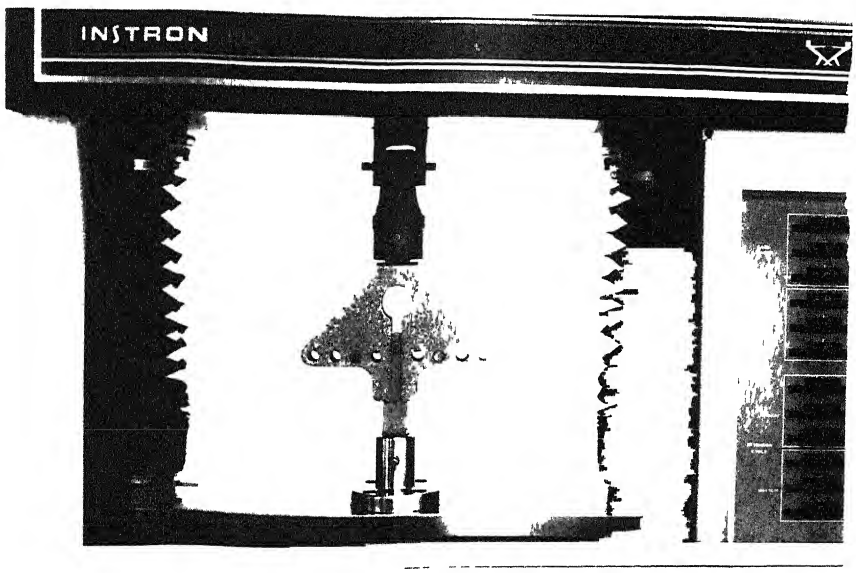

Fig. 3.2(b) ENF test set-up.

CHAPTER 4

IMPACT ON COMPOSITE LAMINATES

4.1 INTRODUCTION

Fibre-reinforced composite materials are being used in many applications which could involve severe impact loading. The suitability of a composite for a particular application is, therefore, determined not only by the usual design parameters, but also by its impact properties.

Many impact tests have been developed for evaluating material toughness or resistance to fracture. The most common tests of Izod and Charpy gives energy to fracture. Limitations to these methods lie in their inability to provide data of basic physical significance. Another method that has been used to study the impact strength of composite is drop weight or the instrumented Avery Izod pendulum impact.

A third method for investigating the response of materials to impact loading is by impacting specimens with various projectiles. There are air guns for firing projectiles and there is the thin flyer plate technique. The advantage of using air gun compared to the previous methods lies in the wide range of projectile velocities that can be generated by the gun.

In the present work impact test has been done on composite laminates using an air gun and a steel projectile in the shape of a cylinder and of hemispherical shaped front.

4.2 FABRICATION OF COMPOSITE PLATE

The composite plates used for impact experiment were fabricated in the laboratory. The details of the raw materials chosen are given below.

Fibre - Fine woven glass cloth (purchased from FGP, Bombay)
Thickness - 0.14 mm
Weight/area - 185 g/m^2
Count/inch - 36x32 /inch
Matrix - Araldyte epoxy LY556 with resin hardener

Sixteen layers of the fibre cloth were used in a laminate to get a plate thickness of about 3 mm with an expected fibre volume fraction of 40%. The test specimens for the measurement of fracture toughness (as explained in Secs. 2.5 and 3.4) also were made of the same materials and constituent volume fractions.

Details of fabrication

The glass cloth was cut from the roll to the required size. Sixteen layers were used for one casting. The plates were fabricated in an open die casting process by hand lay up. Two polished flat steel plates of 25 mm thickness were used as dyes. Two mylar sheets (of thickness 0.05 mm) were used to

avoid sticking of resin with the surface of the plates. The required quantity of epoxy and hardener (10% by weight of epoxy) were weighed. The epoxy was kept in the heater for some time to remove the moisture. The plate and the mylar sheets were cleaned with acetone. The tools necessary for casting such as the metal roller, the brush and the rubber roller were also kept clean. Four metallic spacers (3 mm thick) were used, to be kept between the plates for getting the required thickness. Wax was applied on the spacers and the portions on and around the bolts and bolt holes in the lower and upper plates. This was to avoid any chance of sticking of epoxy with the metal surface.

The heated epoxy was cooled to the room temperature by keeping in ice cold water for some time. The hardener was slowly poured to the epoxy and thoroughly mixed taking care not to create air bubbles, by stirring properly. On the lower dye plate a mylar sheet was laid. Holes were already made in the mylar sheets to fit in the four bolts at the corners of the lower dye. With the brush a thin layer of resin was applied on the mylar sheet over which the first layer of glass cloth was placed. A metal roller was applied on this to spread the resin uniformly and to remove any air bubbles. The process of applying the resin, laying the cloth and using the roller was repeated in the above order till all the layers were laid. Identical fibre alignment was maintained in all the layers. Throughout the casting care was taken to apply sufficient resin to have proper wetting. A mylar sheet

was kept at the upper side also and the spacers were placed at the corners of the plate. A long rubber roller was applied slowly with pressure from the centre towards the edges of the plate to squeeze out excess of resin and to remove trapped air. It was necessary to remove excessive resin, which otherwise would cause slipping between the plies. Now the upper die was gently kept over the lay up and the plates were fastened together tightly to get the required pressure. Care was taken to have uniform tightening of the nuts. The nuts at the opposite corners of the plate were tightened. Also excessive tightening was avoided to eliminate the bending of the steel plates (which can cause variation in thickness of the composite plate) and slipping of plies.

After six hours the heater attached to the plates was switched on for twelve hours. The heater maintained a temperature of about 55^{o}C as a low current was applied to it through a previously set dimmerstat. The heating helped to improve properties such as toughness. The curing time was twenty four hours.

The plate was removed after curing and cut to the required size using a diamond wheel cutter. The edges of the cut pieces were smoothened by rubbing on a sand paper. Two square plates of size 180x180 mm were cut from a single casting.

4.3 EXPERIMENTAL TECHNIQUES FOR CLAMPED PLATE IMPACT TEST

For impacting composite panels with a projectile a gun is

required which can accelerate a projectile to the required velocities. Also, the velocity of the projectile should be measured accurately just prior to the impact. Further, the target panel should be supported rigidly on the mount.

The air gun available in the laboratory was used for conducting experimental studies of balistically impacted composite laminates. The breech assembly which stores high pressure nitrogen gas is equipped with a quick opening mechanism as well as the control panel to fire. The gun barrel has 11 mm bore and is 3.65 m long to obtain high velocities. These velocities can simulate the velocities of bullets fired from regular guns. The long barrel is made of a seamless steel pipe and is supported at five places as shown in Fig. 4.1. Since the barrel is very long and of small diameter it's internal surface is not machined. Therefore, it was polished by wrapping sand papers of various grades starting from coarse to fine on a wooden plug and pulling it in and out of the barrel.

The air gun has several advantages over the conventionally used gun (i) projectiles of varying lengths can be used in the air gun (ii) its projectiles can be made of different kinds of materials such as steel, aluminium, lead, plastics, stones etc. (iii) the shape of the projectile nose can be made hemispherical, conical, flat or of other curvature and (iv) the velocity of the projectile can be varied from a very low velocity of 15 m/sec to supersonic velocities.

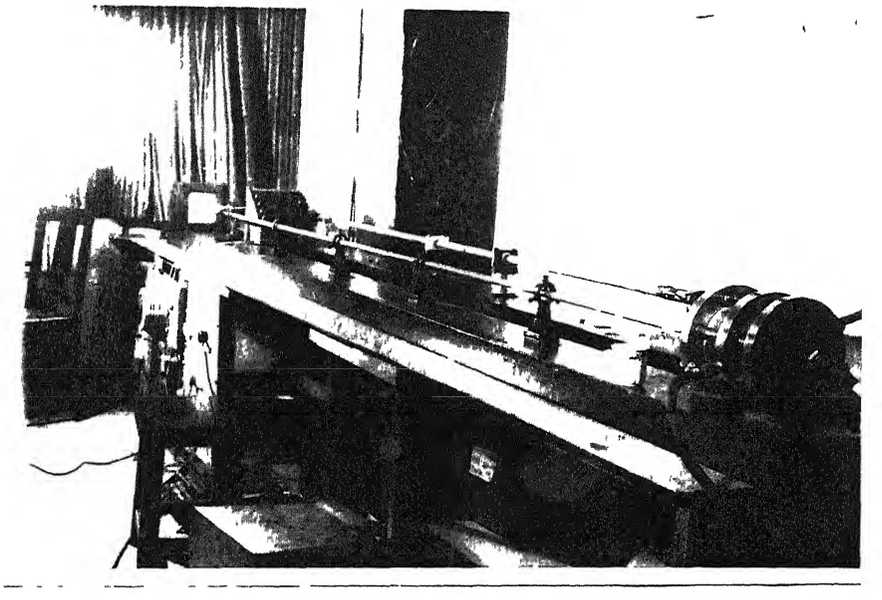

Fig. 4.1 The experimental set-up for impact on clamped panels

In this study a cylindrical projectile of 20 mm length with hemispherical nose has been chosen as shown in Fig. 4.2. It is made of mild steel weighing 116 gm. In order to prevent leaking of compressed nitrogen gas through the sides of the projectile, an 'O' ring has been inserted on a suitably designed groove close to the rear end. The 'O' ring is kept lubricated with the silicone vacuum grease.

The velocity of the projectile coming out of the barrel is measured through an optical system. Three light beams are emitted, from IEE 387 bulbs installed at the intervals of 25 mm within a rectangular shaped steel block attached at the end of the barrel (Fig. 4.3). Each light beam is received by a photodiode (SI 100) embedded on the other side of steel block such that the projectile passes between the bulb and the photodiode. These photodiodes are connected to a time counter capable of measuring time with an accuracy of 1 μs. As the projectile cuts the first light beam, first window of the counter starts counting; when the projectile cuts the second beam, the first window of the counter stops and the second window starts counting time for the time taken by the projectile to travel from second to third light beams. Thus by knowing the distance between the light beams and time taken by the projectile, the velocity is determined. For each shot the bullet was inserted through the front of the gun barrel and it was pushed backwards through the barrel using a stiff metal wire till the bullet reached the rear end of the barrel.

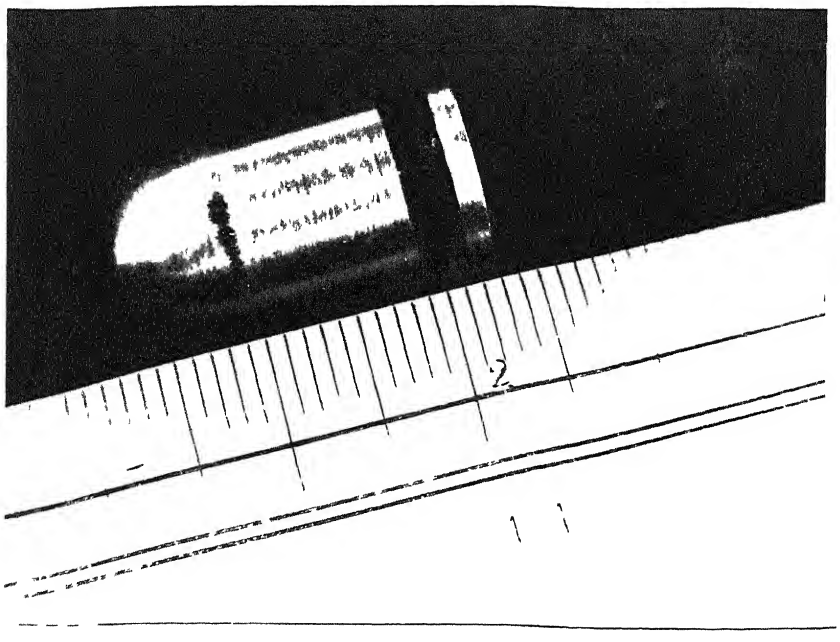

Fig. 4.2 The projectile

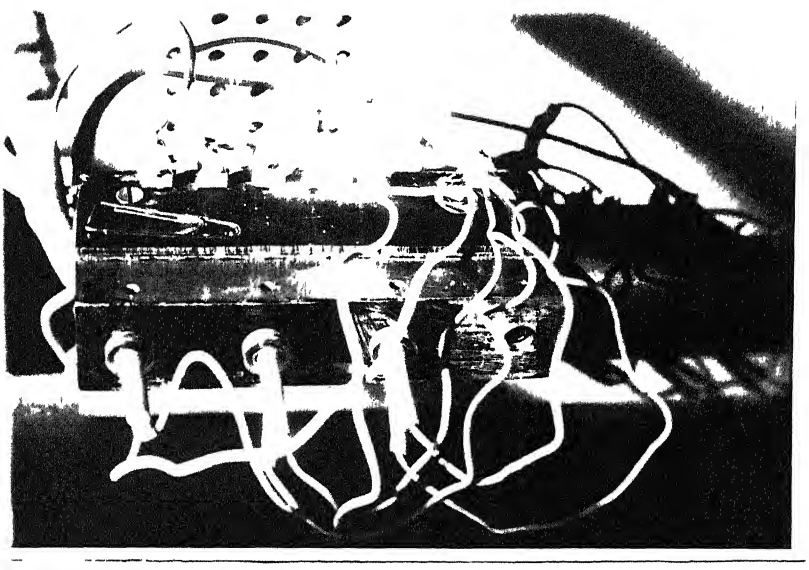

Fig. 4.3 Projectile velocity measurement system

The available chart of nitrogen pressure versus bullet velocity (Fig. 4.4) was used to get the desired impact velocity by suitable setting on the control panel.

The mount to hold the target plates (laminates) is designed to withstand the impact of a long projectile of 75 mm length hitting it with supersonic velocity of 400 m/s. The target plate is clamped between two rigid squared shaped rings to hold 180x180 mm laminates (Fig. 4.5). (These are typical dimensions of sheets supported on the structure of an aeroplane, such as between bulk heads and stringers). For high speed projectiles penetrating through the laminates, a cylinder catcher fitted with cotton rags is placed just behind the target plate.

4.4 ENERGY DISSIPATION IN IMPACT

There are various ways by which the incident energy of the impactor gets dissipated. This can be expressed as

$$E = E_f + E_s + E_r + E_d + E_o$$

where

E - total energy of the impactor

E_f - energy lost in fluxural vibration

E_s - energy absorbed in the support

E_r - rebound energy of the impactor

E_d - energy dissipated in the damage zone

E_o - any other form of energy dissipation such as noise

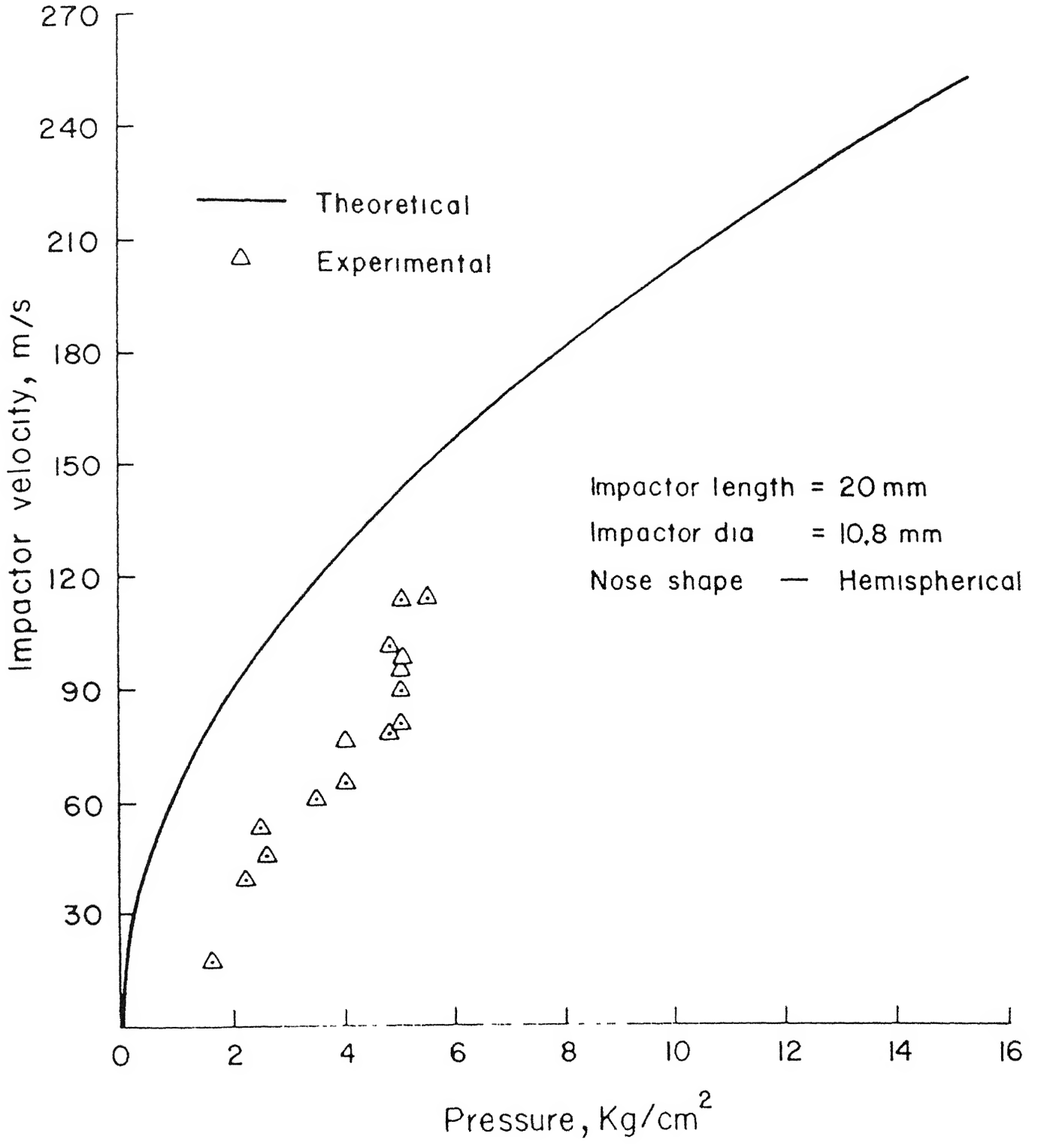

Fig. 4.4 Impactor velocity versus pressure

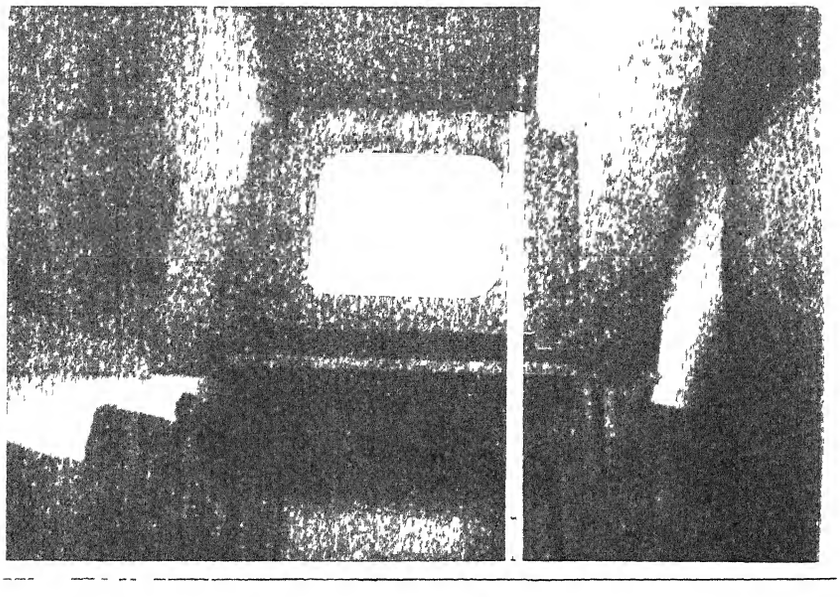

Fig. 4.5 Panel holder

The term E_d can be again divided into different forms as

$$E_d = E_{fb} + E_{del} + E_{mc} + E_{do}$$

where

E_{fb} - energy dissipated in fibre breakage

E_{del} - energy dissipated in delamination

E_{mc} - energy dissipated in matrix cracking

E_{do} - any other form of energy dissipation such as debonding

The energy lost in fibre breakage is low since the fracture energy of brittle fibres are low. The energy dissipation in the matrix cracking is also low since the total damage area is small. The delamination energy losse is considered to be high because of the large crack surface areas created in the process. None of these energies are directly measurable. In the present study the interest is to find the fraction of the energy of the impactor dissipated in delamination.

4.5 DAMAGE MEASUREMENT

Several different methods have been used to identify the damage in an impacted laminate. Among the nondestructive methods c-scan, ultrasonic, x-rays, die penetration, viewing the laminates against luminous background have been used. These methods identify the total damage easily, but they do not provide much information about the damage configuration inside the material.

In order to figure out the distribution of delamination on the different interfaces of the laminate and hence to find out the total delamination area, a destructive technique has been adopted. Most common among the destructive techniques is the thin strip method. The damaged laminate is cut on a diamond wheel cutter into thin strips and the cross sections are polished to observe the damage through the thickness.

To get the delamination area on each interface the size and shape of each area should be found. This is difficult mainly because the size of delamination zone is relatively small and also because the cutter removes considerable material (about 2 mm width). Thus the delamination area had to be found in an approximate way. The impacted laminate was cut through the point of impact into two parallel strips on a diamond cutting machine using a thin cutting blade. The damaged portions were cut and removed from the main plate to get two thin strips from a target plate. The cross sections were then polished with very fine sand paper. Using a travelling microscope the average length of delaminated interface (total of 15 interfaces in the 16 layered laminate) was measured. The dimensions measured are indicated in Fig. 4.6. The impacted side of the laminate appear to have square shaped delamination and the rear side, corner rounded square. As an approximation square shaped damage was assumed throughout and the total delamination area was obtained as

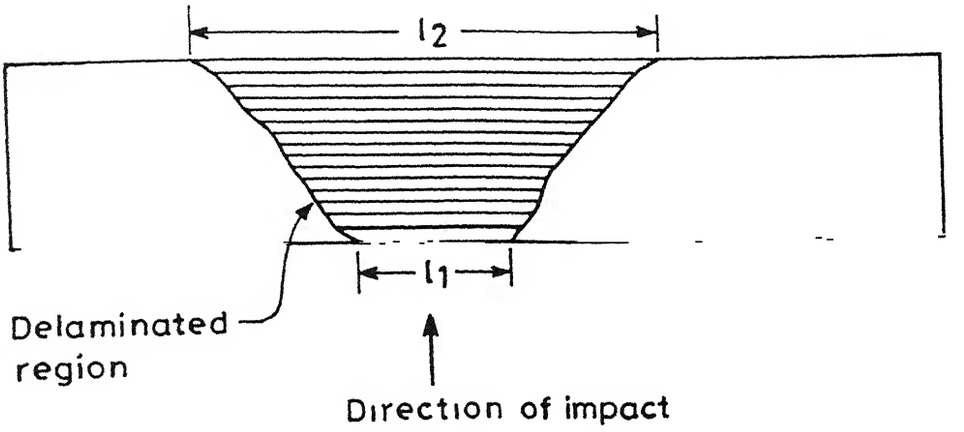

Fig. 4.6 The cut section view of an impacted laminate.

$$A_{del} = \frac{1}{2} \left(\frac{l_2^2}{2} + \frac{l_1^2}{2}\right) \times 15$$

This area was found for both the strips and average value was taken.

4.6 IMPACT ON HANGING PLATE

As mentioned in Sec. 4.4 a part of the incident energy of the projectile gets absorbed in the support on which the target is mounted. This is because the target plate is clamped on a foundation which is actually not rigid. This energy is absorbed in the elastic deformation of the support. This energy cannot be assessed easily. Also there will be a rebound energy for the projectile after impact. This also is not obtained from the experimental set up.

To get the amount of energy that gets dissipated in the plate a simple hanging plate experiment was devised.

The purpose of this experiment is to find the fraction of impact energy that actually gets absorbed by the composite plate.

The impacting target plate used was the same as that used in the clamped plate experiment. A frame for the suspension of the plate was fabricated for the purpose. The plate was hung by two inextensible threads, thus its edges were free. The

centre of the plate was adjusted to be in line with the centre line of the gun barrel. The experimental set-up is shown in Fig. 4.7. The details of its fabrication is given in Sec.4.7.

When the bullet is shot, a part of the momentum of it is transferred to the plate and it swings like a pendulum about the suspension line. The final position corresponding to the maximum potential energy (or zero kinetic energy) of the plate is marked on a transparent sheet by visual observation of the plate position when it comes to momentary rest.

Determination of panel velocity right after the impact

Applying the conservation of momentum to two states of the system (laminate panel and the projectile) before and after the impact, we have

$$mv_1 + MV_1 = mv_2 + MV_2 \qquad (4.1)$$

where

- m - mass of the bullet
- M - mass of the plate
- v_1 - incident velocity of the bullet
- v_2 - rebound velocity of the bullet
- V_1 - velocity of the plate before impact
- V_2 - velocity of the plate after impact

Velocity V_2 of target plate after the impact is determined by observing the height H to which the plate rises. If the wind

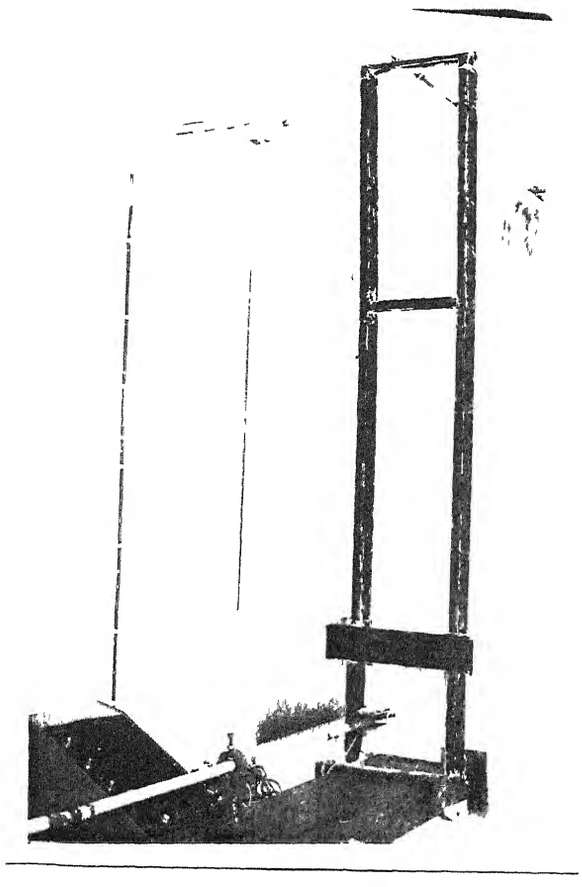

Fig. 3.7 Experimental set-up for the hanging plate impact

drag on the panel is neglected, V_2 is obtained in straightforward manner by equating the potential energy of the plate to the kinetic energy after impact.

$$\frac{1}{2} MV_2^2 = MgH$$

or

$$V_2 = \sqrt{2gH} \tag{4.2}$$

Substituting Eq. (4.2) in Eq. (4.1) and noting that $V_1 = 0$ we get

$$v_2 = \frac{mv_1 - M\sqrt{2gH}}{m} \tag{4.3}$$

and thus the fraction of energy absorbed in the system is

$$f = E_p/E$$

where

E_p = energy absorbed by the plate

$= E - E_{KE} - E_r$

where

E - impact energy of the bullet, $1/2\ mv_1^2$

E_{KE} - kinetic energy of the plate after impact, $1/2\ MV_2^2$

and E_r - rebound energy of bullet, $1/2\ mv_2^2$

The fraction of energy absorbed 'f' is found as a function of velocity of bullet v_1.

The drag due to air resistance can reduce the height to which the plate moves. This was also accounted and the corrected value of V_2 was used in Eq. (4.3) in place of '$\sqrt{2gH}$.' The details of finding out the energy loss due to drag is given in Appendix C.

4.7 EXPERIMENTAL SET UP FOR HANGING PLATE IMPACT

A 3/4 inch thick perspex sheet was used for the fabrication of the frame (Refer, Fig. 4.7). The sheet was cut into the required sizes in an all cut machine and the cut pieces were joined by applying liquid chloroform. In the topmost horizontal bar, a slot was made for the position adjustment of the plate. The base of the frame was made wider in the direction of impact to take up the bending moment. The frame was kept in such a way that the channel on which the gun barrel is mounted was fit inside the frame, the bottom of the frame touching the table. A 'c' shaped metallic clamp with screws on one side was used to fasten the frame with the channel.

The motion of the impacted plate was viewed through a thin perpex sheet kept vertically on one side of the channel, on the table. The path of the plate's motion was marked on the perspex sheet for easy reference. The composite plate was suspended by two twine threads. For this purpose two holes were drilled in the plate. Before impacting, the plate was centered properly.

CHAPTER 5

RESULTS AND DISCUSSION

The interlaminar fracture toughness tests were conducted for mode I and mode II failures on specimens made of glass fabric reinforced laminates. Impact tests were conducted on the same laminates in two ways, i) clamped plate, and ii) hanging plate as the support conditions. The experimental results and discussions are given individually in this chapter.

5.1 MODE I INTERLAMINAR FRACTURE TOUGHNESS

As described in Chapter 2 the force-displacement diagram was obtained for the mode I interlaminar test. One such diagram is shown in Fig. 5.1 for DCB specimen No.4. The plots for other samples are similar. Details of the experimental values and the results are given in Table 5.1.

The following observations can be made from the graph. They are mostly in agreement with the works of others [3,6-8, 21-22].

The compliance of loading curves increases with crack length. This is because the specimen becomes less stiff as the crack propagates. The compliance-cracklength plot for the specimen is given in Fig. 5.2.

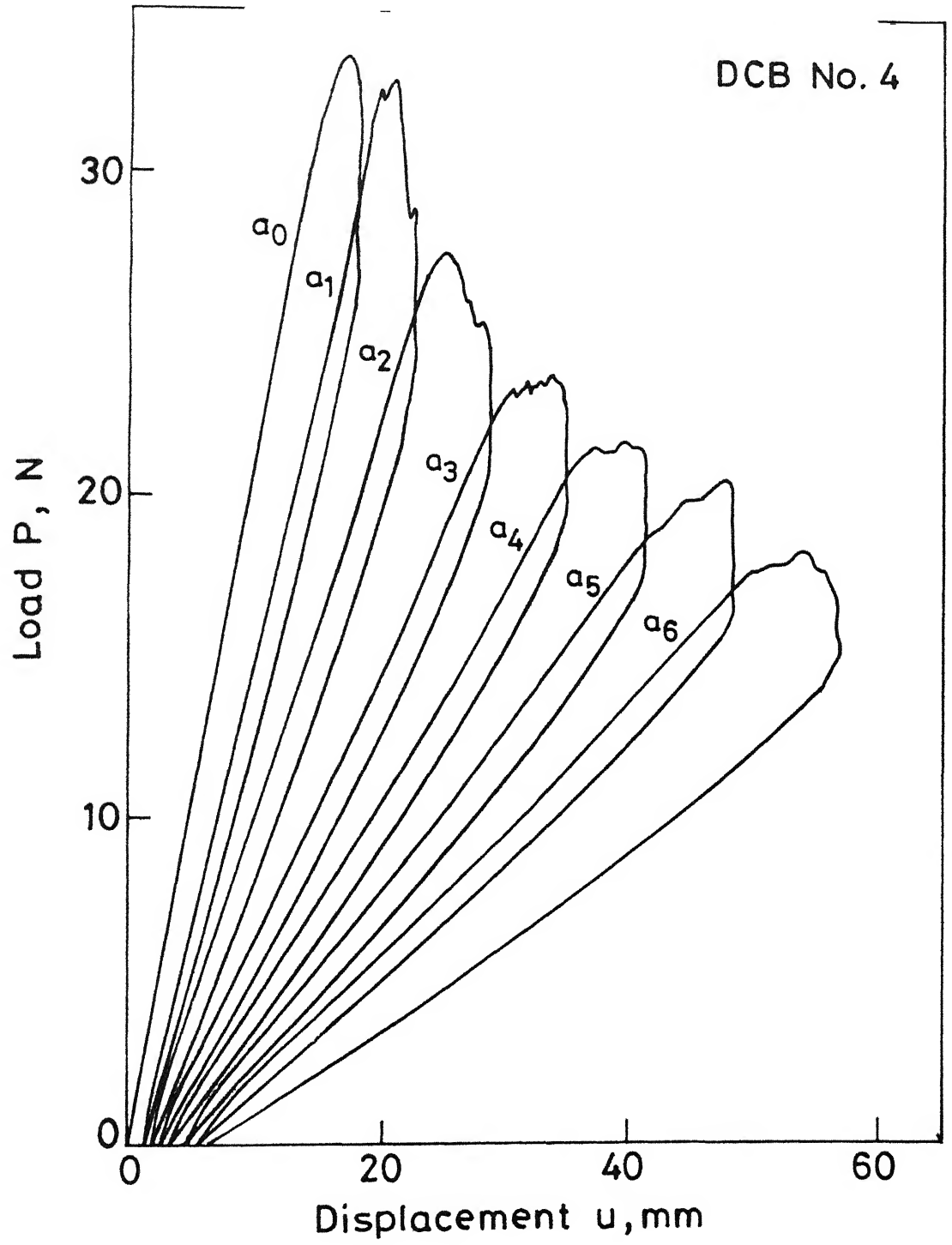

Fig. 5.1 A typical load-deflection curve of DCB test.

Table 5.1 Result of DCB Tests

DCB No.	Thickness mm	Range of crack length tested mm	No. of cycles	Critical energy release rate G_{IC}, J/m^2				
				Compliance method	Using formula	Area method	Modified area method	Nonlinear theory
1	2.9	58-88.5	5	687	683	778	649	676
2	2.9	42-91.5	6	725	712	951	597	781
3	3.0	42.5-98.5	7	712	785	860	651	710
4	2.9	38-85.5	7	691	729	925	584	688
5	2.6	37-84	5	678	720	716	627	671

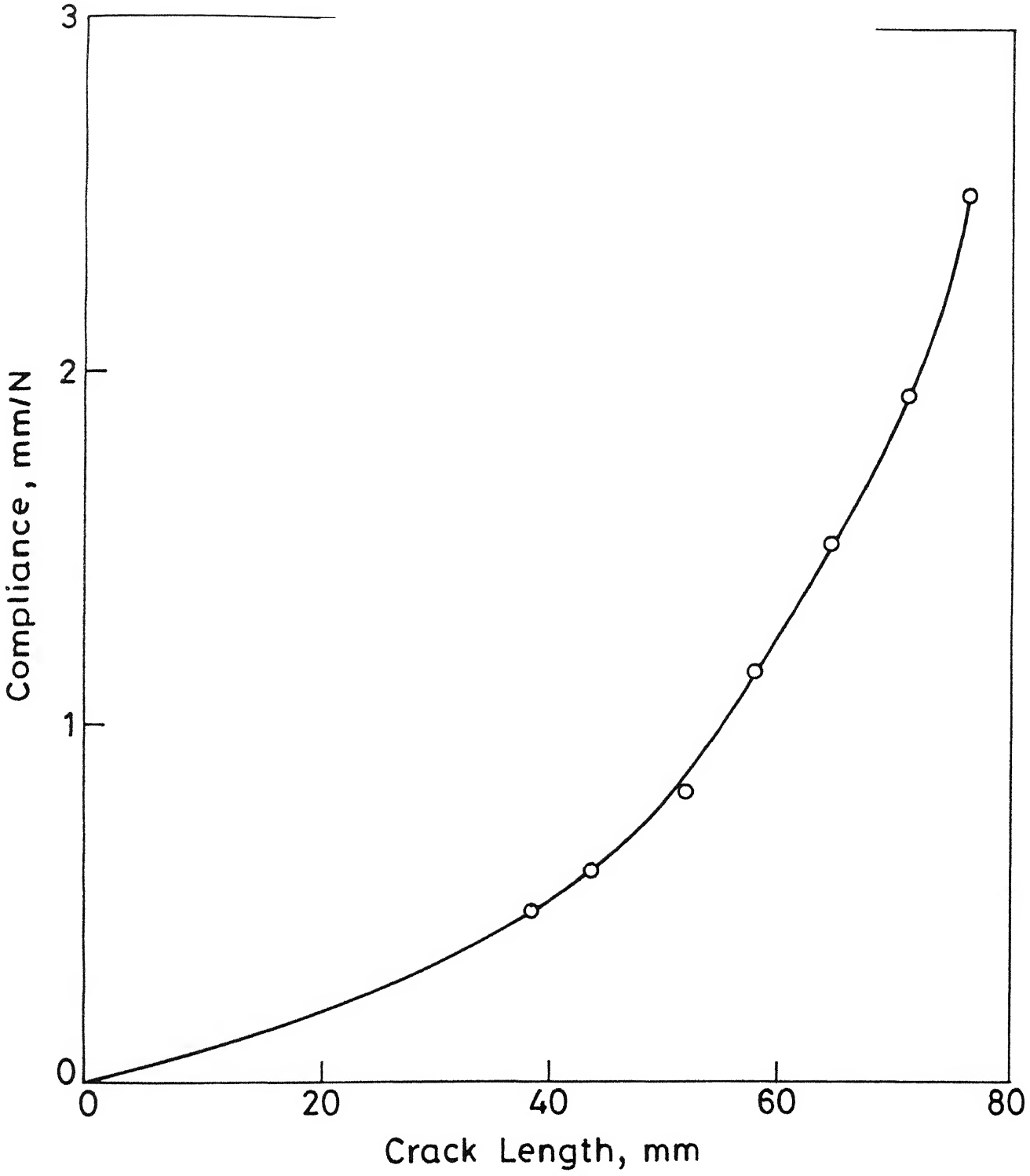

Fig. 5.2 Variation of compliance of the DCB specimen No. 4 with crack length.

The critical load for the crack initiation versus the crack length is shown in Fig. 5.3. As expected the load decreases with increase in crack length as the effective moment arm for the applied force on the crack front increases.

The loading curve corresponding to any crack (Fig. 5.1) lies above the unloading curve of the preceeding crack, which means that there is hysterisis loss in every cycle.

When the machine is switched off after the crack propagation, it is seen that there is a drop in the load with time. This is due to the viscoelastic behaviour of the material.

The critical displacement u_c (corresponding to the critical loads) is plotted against the crack length 'a' in Fig. 5.4. It may be noted that the ratio u_c/a increases with crack length, tending towards large deflections. At the long crack lengths the fracture energy may strongly depend on the plastic behaviour of the beams, especially for beams of small height [8]. Thus, it is important to avoid testing at large crack lengths.

When the specimen is unloaded to zero load a permanent deflection is observed. Its magnitude is 5 to 15% of the maximum critical displacement for the largest crack length making it visually evident. A plot of permanent deflection versus crack length (Fig. 5.5) shows a general trend. The permanent deflection goes on increasing with the crack length.

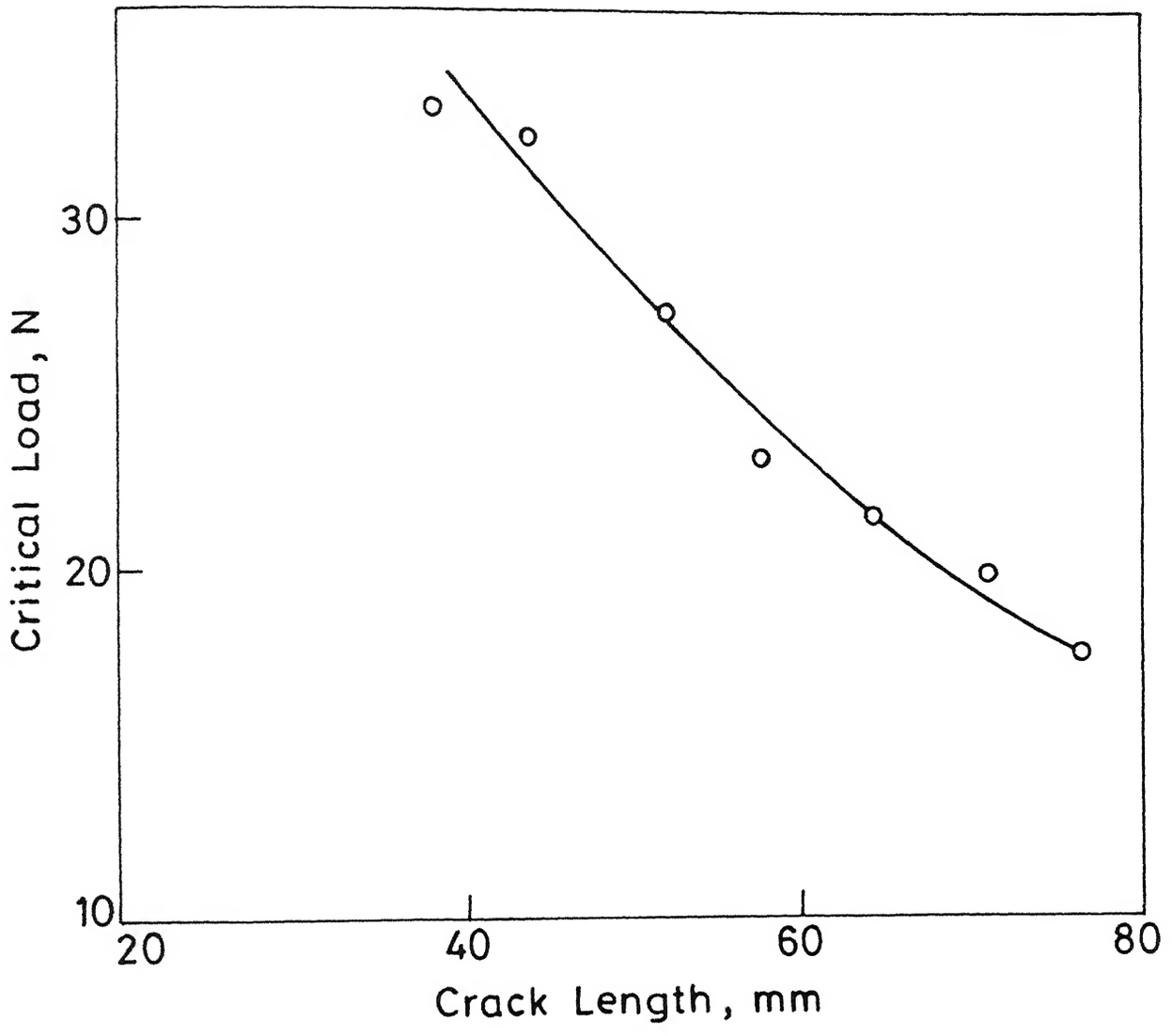

Fig. 5.3 Critical load - crack length curve for DCB specimen No. 4.

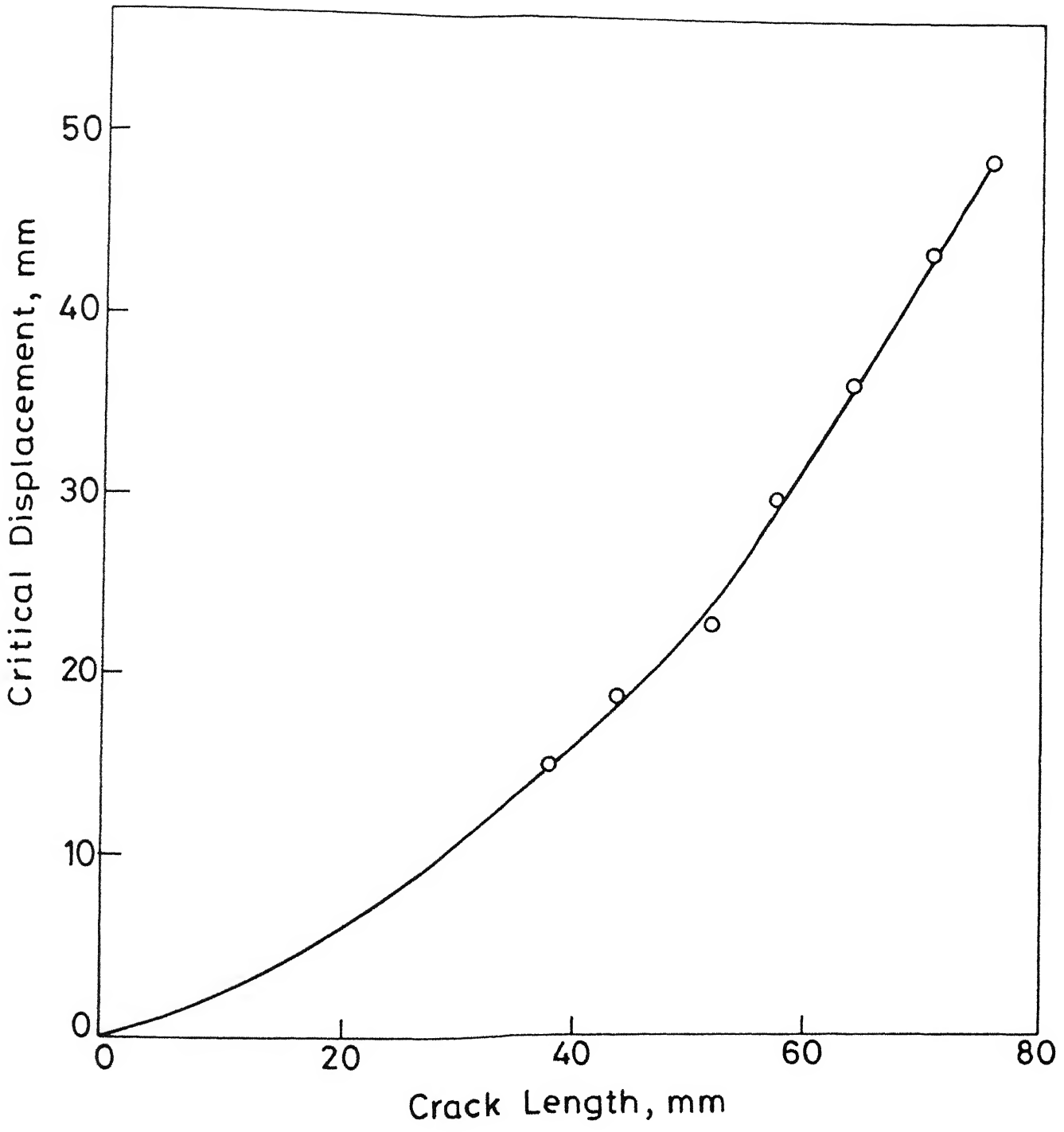

Fig. 5.4 Variation of critical displacement with the crack length of DCB specimen No 4.

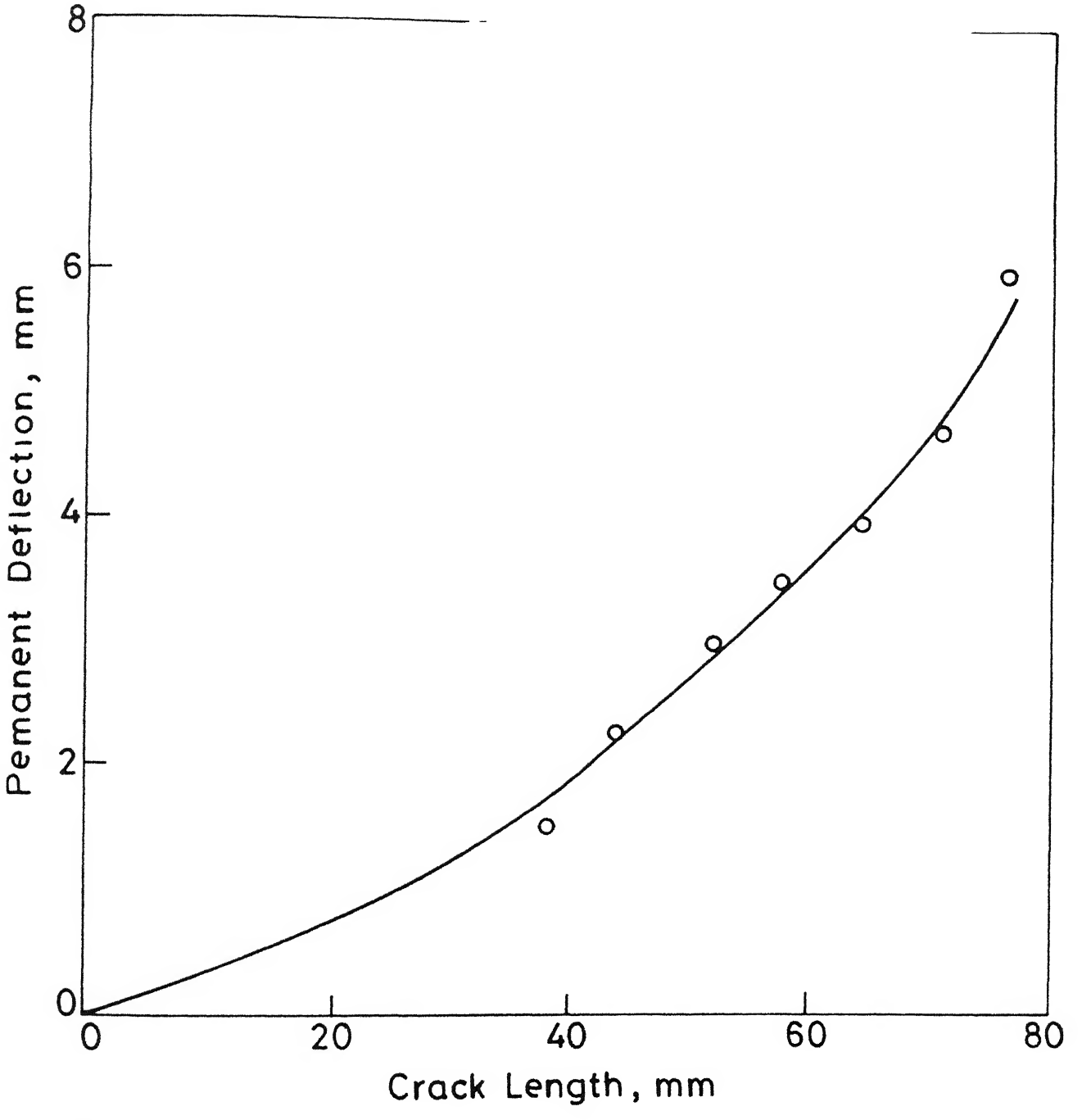

Fig. 5.5 Permanent crack opening displacement vs crack length for DCB specimen No. 4.

Since the beam used is slender, the deflection is considerably large and the outer layers of the beams probably get stretched beyond elastic limit causing permanent deformations. This can also be due to damage at the crack tip causing a permanent crack opening displacement. It should be emphasised that permanent deflection is a cumulative parameter of which only a small increment adds during individual tests. Hence, the failure energy is primarily elastic with only a small inelastic component [6].

The log-log plots for finding G_{IC} by compliance method is shown in Fig. 5.6. The average value of G_{IC} calculated by this method is 699 $\pm$ 17 J/m^2.

To get a comparison between the various methods of finding G_{IC}, a plot of G_{IC} versus the specimen number for different data reduction methods are given in Fig. 5.7.

As seen from the figure, the area method gives largest values of G_{IC}. The area method gives larger values of G_{IC} because of the inelastic deformation in the specimen. This is in agreement with as reported by Carlsson and Pipes [20]. Thus, this method cannot be considered as a good method for evaluation of G_{IC}.

The modified area method gives lower value than the area method as expected since the permanent deformation is taken care of. But this method gives lowest values among all methods

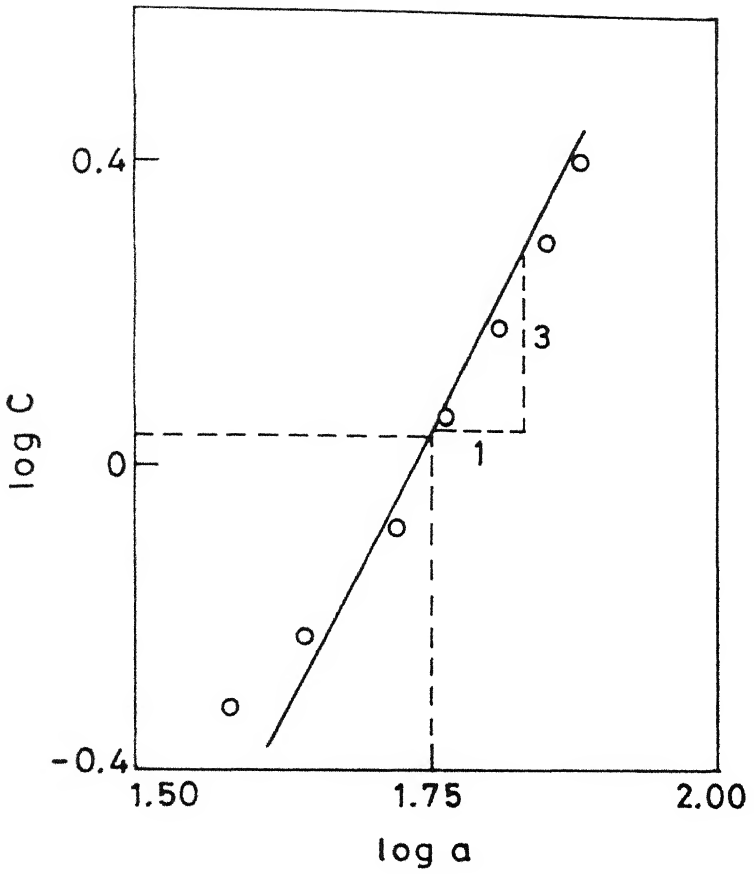

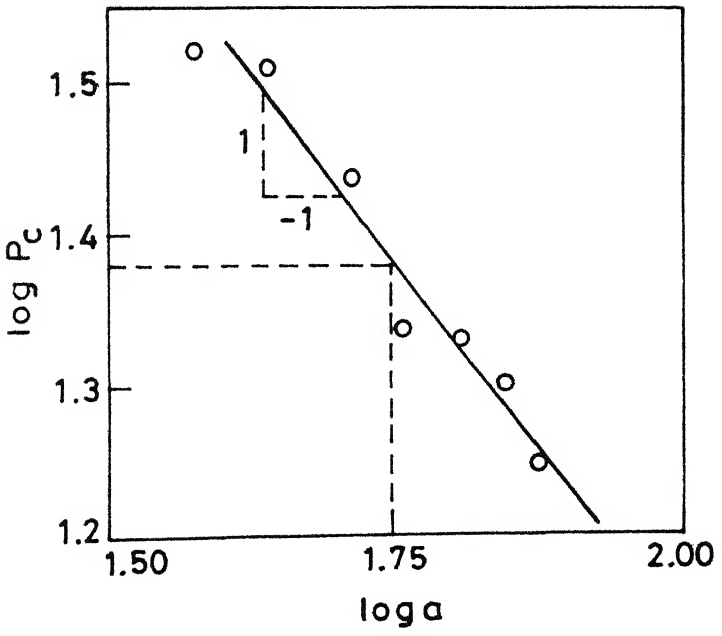

Fig.5.6 log-log graphs for finding A_1 and A_2 (DCB-4)

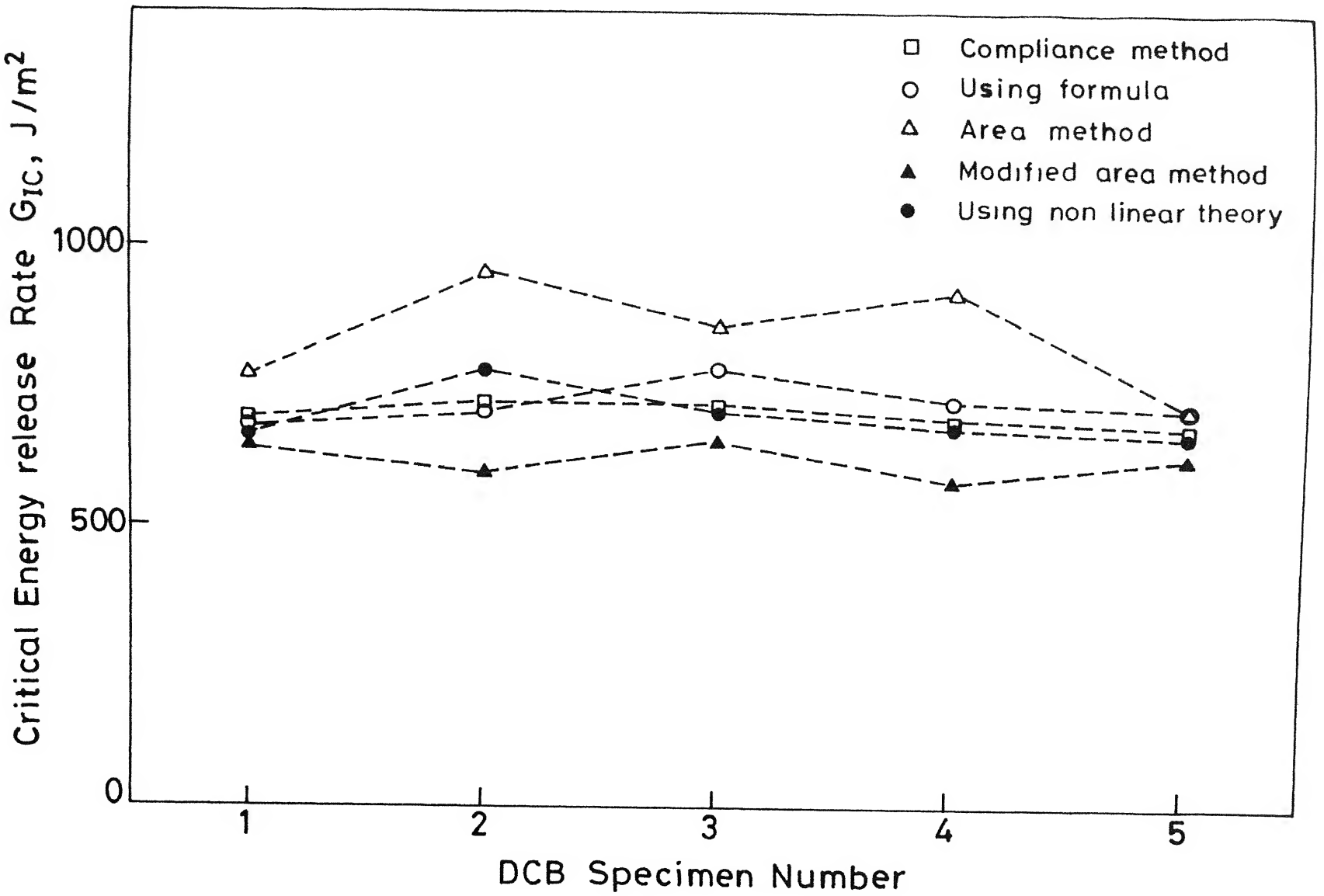

Fig. 5.7 Comparison of mode I energy release rate found by different methods

including the nonlinear theory. After examining the cause of this,the following explanation can be given. As mentioned earlier, it is observed that the loading curve for any crack lies above the unloading curve for the same crack length. Also it is seen that the loading curve is steeper in the initial portion (close to zero load) as shown enlarged in Fig. 5.8. This large difference in slope could be due to some testing machine related error (Note that this apparent machine error will not affect the results of other methods). This will create deviation of the loading curve from the preceeding unloading curve. Thus, the method of moving all the loading curves to a common origin and measuring the areas between them gets defeated, by giving rise to lower values of G_{IC}. Thus, this method has to be discarded for the measurement of G_{IC}.

The compliance method and the method using nonlinear beam theory give values close to each other. Except for DCB No.2 the nonlinear theory values of G_{IC} are slightly lower than that obtained by compliance method. It shows that the nonlinearity in the specimen during the test is negligible. The formula method gives a quick check to the values obtained by other methods. Its value is close to that of compliance method.

As there is difference between various methods, the best method has to be chosen for the calculation of G_{IC}. The compliance method which is more commonly used is taken as the

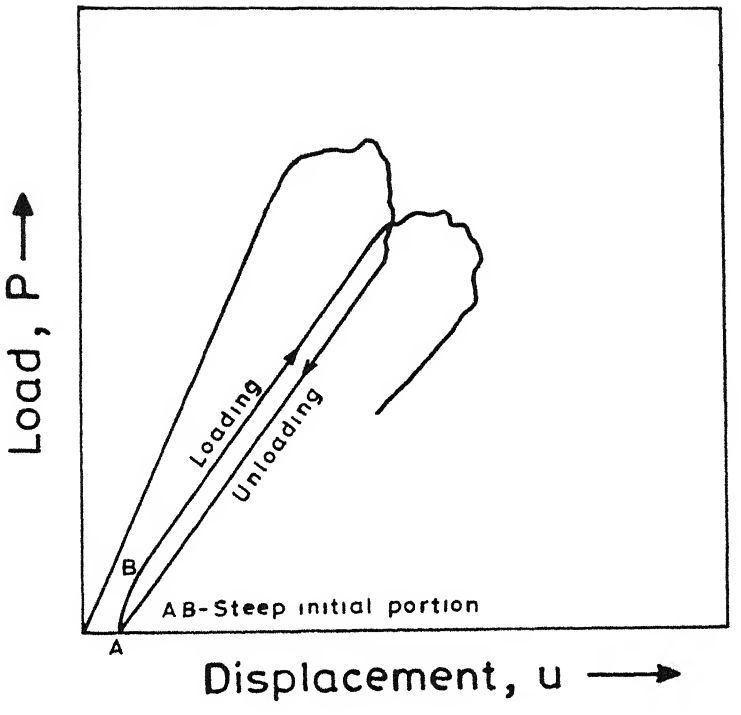

Fig. 5.8 Error in the initial portion of the loading curve in DCB test.

best data reduction method as it gives close value to that of nonlinear theory. Thus the average value of G_{IC} calculated by the compliance method is chosen as the mode I interlaminar fracture toughness of the material.

The variation of G_{IC} is plotted against Δa in Fig. 5.9. Graphs using the formula method and the nonlinear theory are shown. It can be concluded that G_{IC} is more or less independent of crack length. This result is in agreement with the findings of S. Hashemi etc. [21,22] though they have used different materials. The area method and modified area method gave highly scattered values and were not plotted. This is another proof of nonreliability of these methods.

5.2 MODE II INTERLAMINAR FRACTURE TOUGHNESS

As explained in Chapter 3 the load-displacement diagram was obtained for mode II fracture toughness test. One such diagram for the ENF specimen No.1 is given in Fig. 5.10. The graphs of other specimens are similar. The curve is slightly nonlinear. For calculating G_{II}, linear theory is assumed.

Compliance of the curve is obtained from the corresponding value at the midpoint of the curve. The Table 5.2 gives the G_{IIC} values of various specimens. The average of the test value 1647 ± 59 J/m^2 is taken as G_{IIC} of the material.

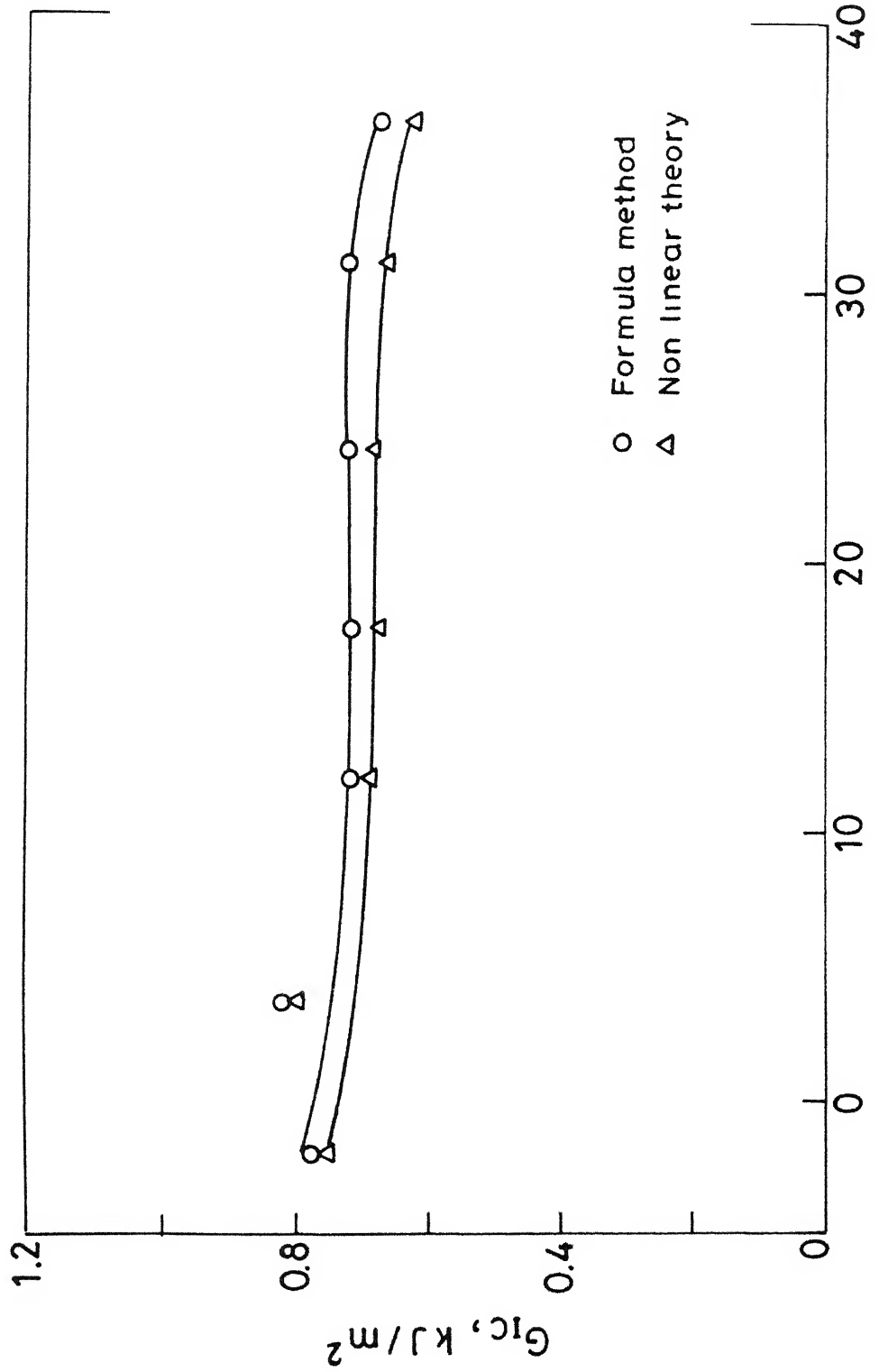

Fig. 5.9 Variation of critical strain energy release rate G_{IC} with Δa for DCB No. 4.

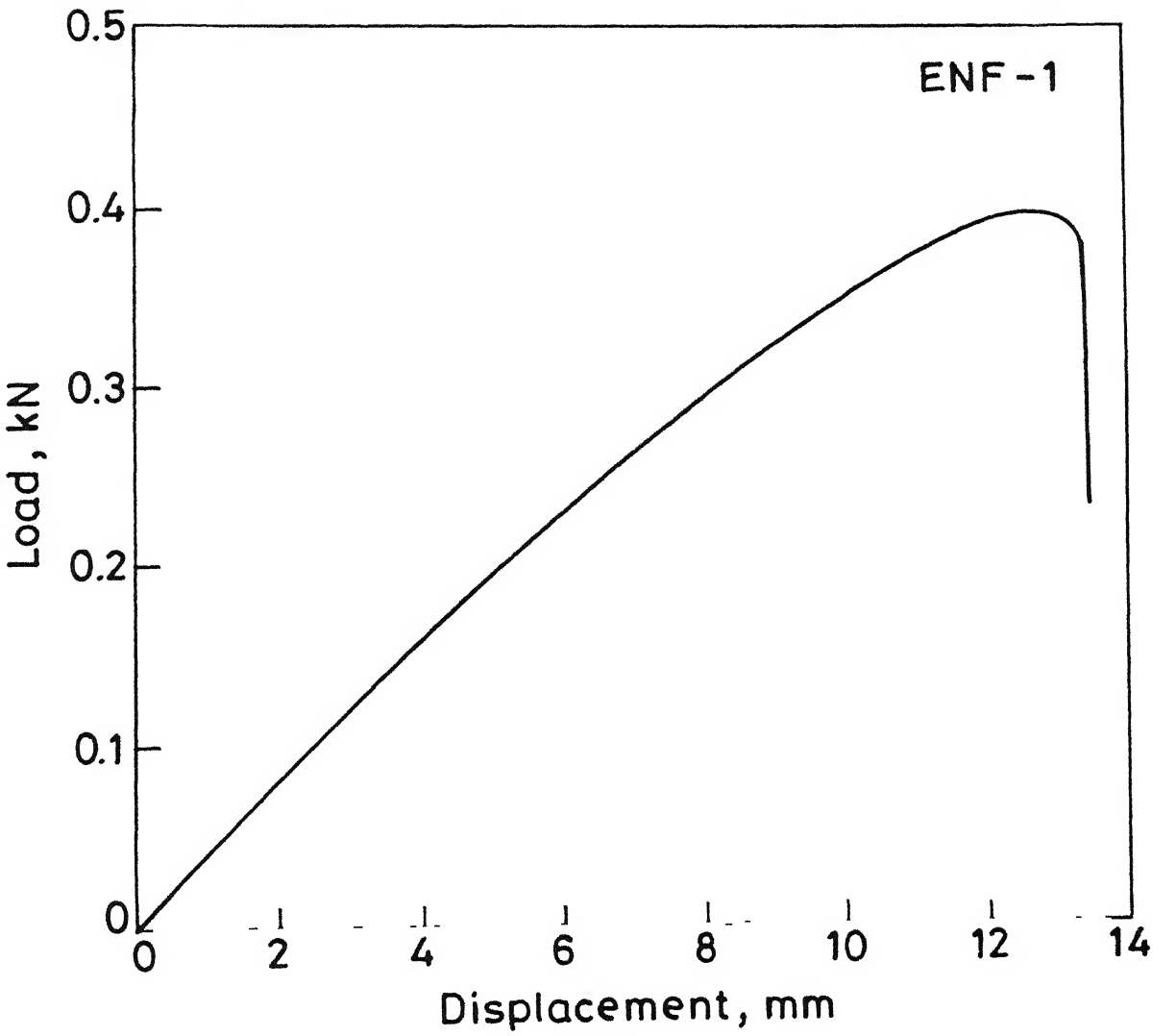

Fig.5.10 A typical load-deflection curve of ENF test.

Table 5.2 Result of ENF Tests

Specimen No.	Thickness mm	Initial crack length mm	Critical load P_c N	Average compliance mm/N	G_{IIC} J/m^2
1	2.8	26	396	0.0275	1629
2	2.8	26	328	0.0373	1558
3	2.6	25	344	0.0408	1689
4	2.6	25	356	0.0398	1710

As explained in Sec. 3.3 it is observed that crack propagates to the central loading point in an unstable manner and during this unstable crack growth there is an instantaneous load drop.

The mode II fracture toughness value is more than twice the mode I value. This is due to more extensive matrix plastic deformation [3] associated with the shear mode compared with the opening mode.

The values of G_{IC} and G_{IIC} obtained in the present study are in agreement with the results of G. Marom et al. [3] for the glass fabric reinforced composites.

5.3 RESULTS OF IMPACT EXPERIMENTS

As explained in Chapter 3, impact experiments were conducted on composite panels of size 180x180 mm.

The delamination area of each impacted plate (as found by the destructive technique)versus the velocity of the bullet is shown in Fig. 5.11. From the test data it appears that the clamped plate and hanging plate responses are similar, thus their results are plotted together. The delamination area increases nonlinearly with the impact velocity. At an impact velocity of 18 m/s, the damage on the plate is barely visible.

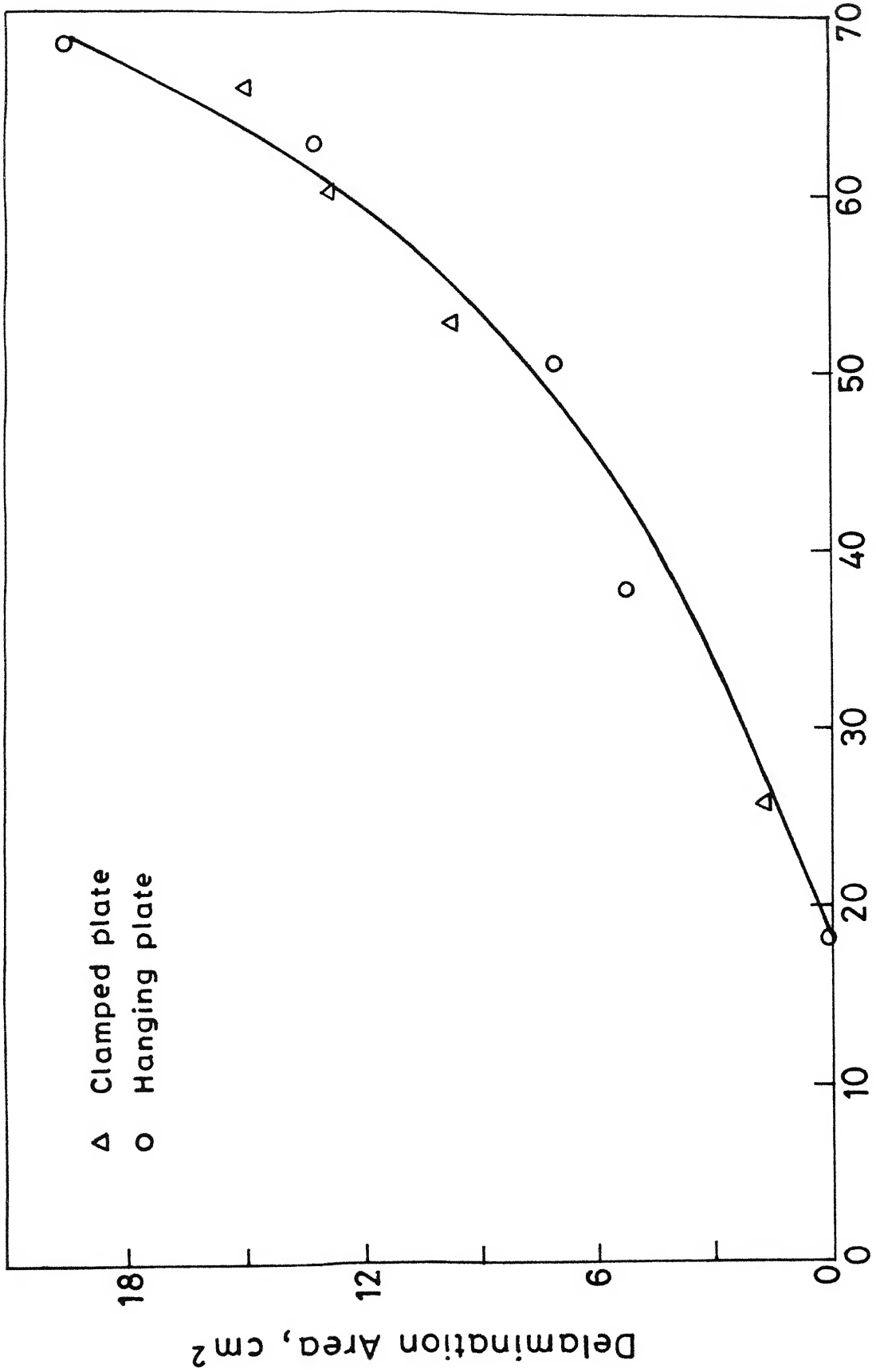

Fig.5.11 Delamination area vs incident velocity of the bullet.

As shown earlier, the total delamination area is evaluated from the impact tests. The results of mode I and mode II tests are applied, to the impact problem. Delamination is caused by the mixed mode (mode I and mode II) interlaminar failure. It is hard to account the contributions of each mode in energy dissipation. Finding the dynamic delamination fracture toughness is complex as seen from the work of J.E. Grady and C.T. Sun [23]. Thus an average value of G_I and G_{II} is taken as the energy release rate (fracture toughness) in delamination due to impact. The average value of G_{IC} (calculated by compliance method) and G_{IIC} is found to be 1173 J/m^2.

The product of the average fracture toughness (as mentioned before) and delaminated area was found to get the energy absorbed in delamination. The results of the impact experiments are given in Table 5.3.

The fraction of energy absorbed in delamination (E_{del}/E) was plotted against impact energy as shown in Fig. 5.12. Certain observations can be made from the graph. There is scatter in the data points. The energy absorbed in delamination increases with the incident energy. The energy dissipated in delamination amounts to the order of 4-9% of the impact energy. This is apparently quite low and contrary to the notion that the delamination is a major energy dissipation mechanism in laminated composites.

Table 5.3 Result of Impact Tests

Sl. No.	Specimen No.	Impact velocity m/s	Impact energy E J	Total delamination cm^2	Energy dissipation in delamination E_{del} (J)	$(E_{del}/E) \times 100$ %
1	12*	18.3	1.97	The damage area barely visible	-	-
2	7018**	26	3.98	1.6	0.188	4.7
3	11	37.76	8.41	5.2	0.605	7.2
4	13	50.5	15.03	7.1	0.827	5.5
5	7016	52.8	16.43	9.7	1.14	6.9
6	7005	60	21.22	12.8	1.5	7.0
7	14	62.65	23.22	13.2	1.55	6.6
8	7004	65.8	25.52	15.1	1.77	6.9
9	15	68.1	27.34	19.6	2.3	8.4

*Hanging plates (two digit numbers)

**Clamped plates (four digit numbers)

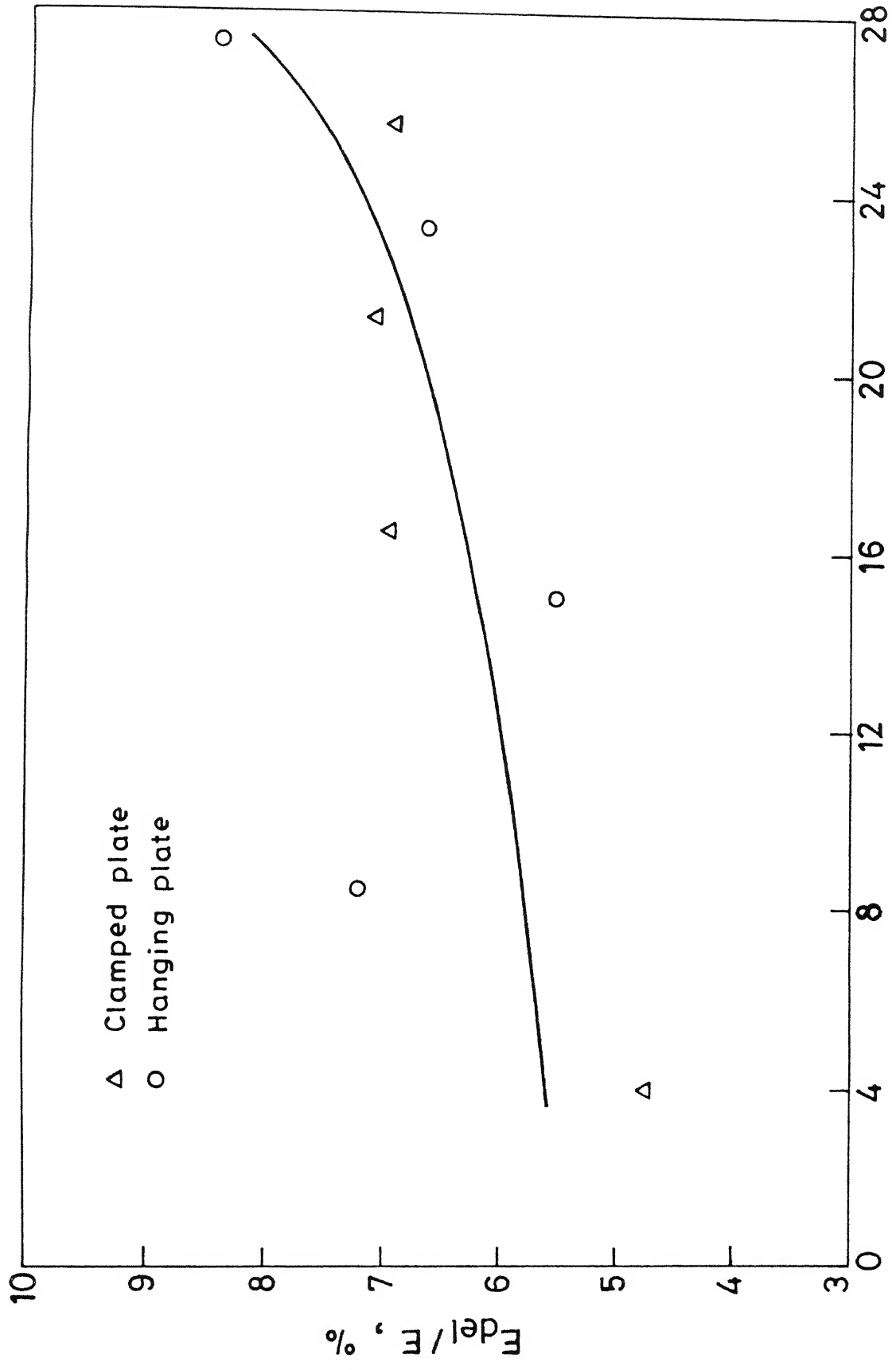

Fig.5.12 Ratio of energy absorbed by delamination and incident impact energy vs impact energy.

It has been observed by many investigators [15,24] that in comparison to the impact side rear side of the panel is damaged more. The finding in this study also supports their observation as it can be seen in Fig. 5.13 where damage on the impact and rear surfaces are shown. The delamination is more at the rear side of the plate as it is clear from Fig. 5.14.

On the rear surface of the impacted panel the fibres are observed to be broken (for higher velocities) due to tensile stress caused by the bending moment. However, fibre breakage occurs only along mutually perpendicular fibre directions (Fig. 5.13). The reason for this is that the tensile stress is maximum on the fibre along fibre directions. In all other directions the fibres are subjected to only a component of the tensile stress. Also the fracture occurs separately on all the four fracture planes around the centre point of impact because they do not join at the same point, thus giving rise to the formation of diagonal fracture planes near the centre. The four fracture planes along the fibre directions behave as transverse cracks they enable delamination cracks to grow on interfaces.

Hanging Plate Impact

The result of the hanging plate impact experiment is shown in Fig. 5.15. The fraction of the energy of the impactor absorbed by the panel is plotted against the impact energy. It shows

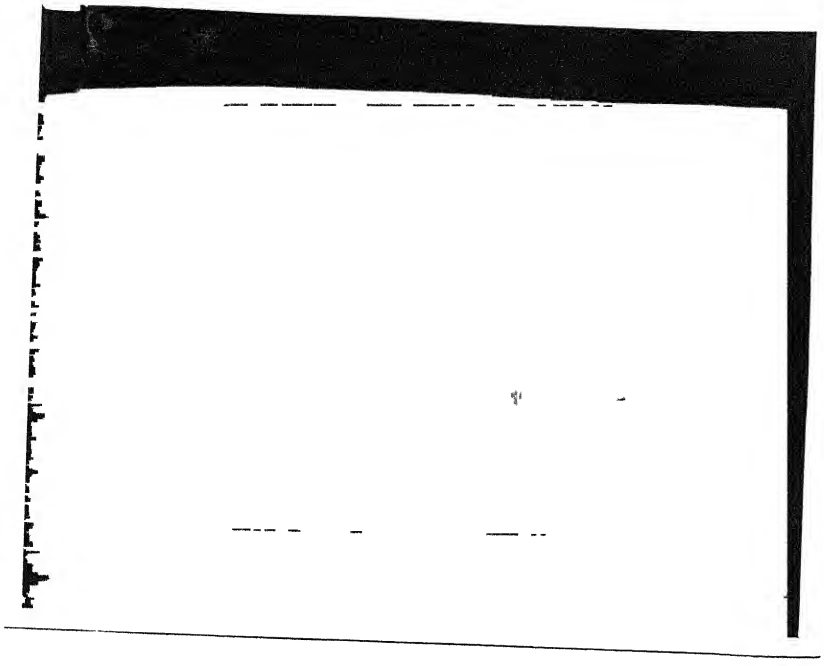

(a) Impact side view

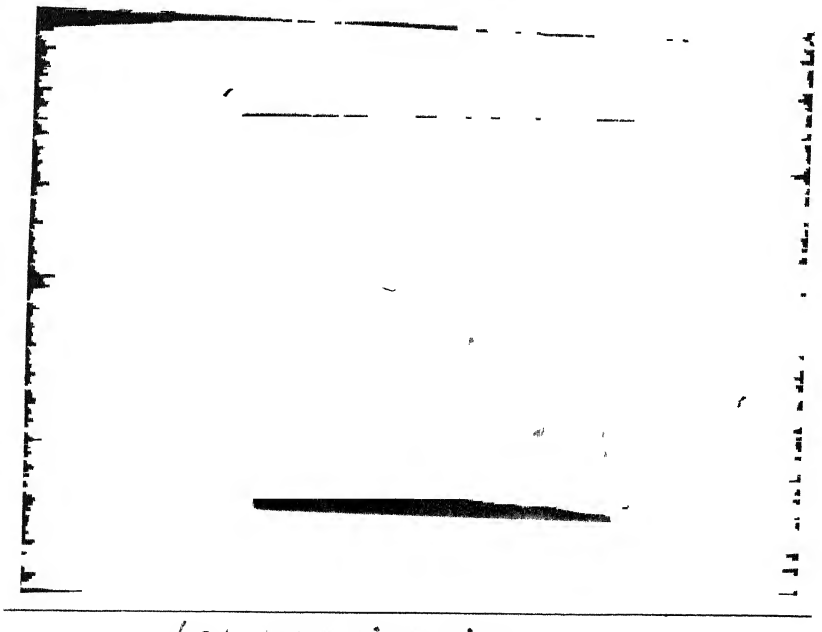

(b) Rear side view

Fig. 5.13 Two views of a damaged laminate

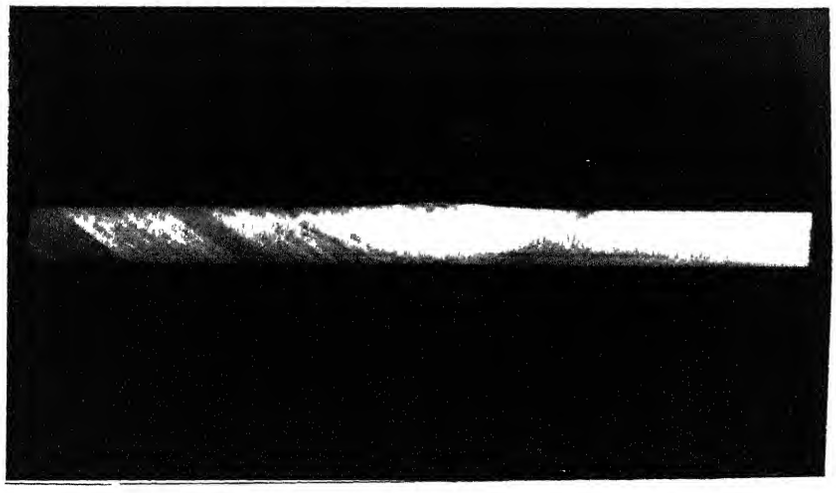

Fig. 3.14 The cut section view of an impacted laminate

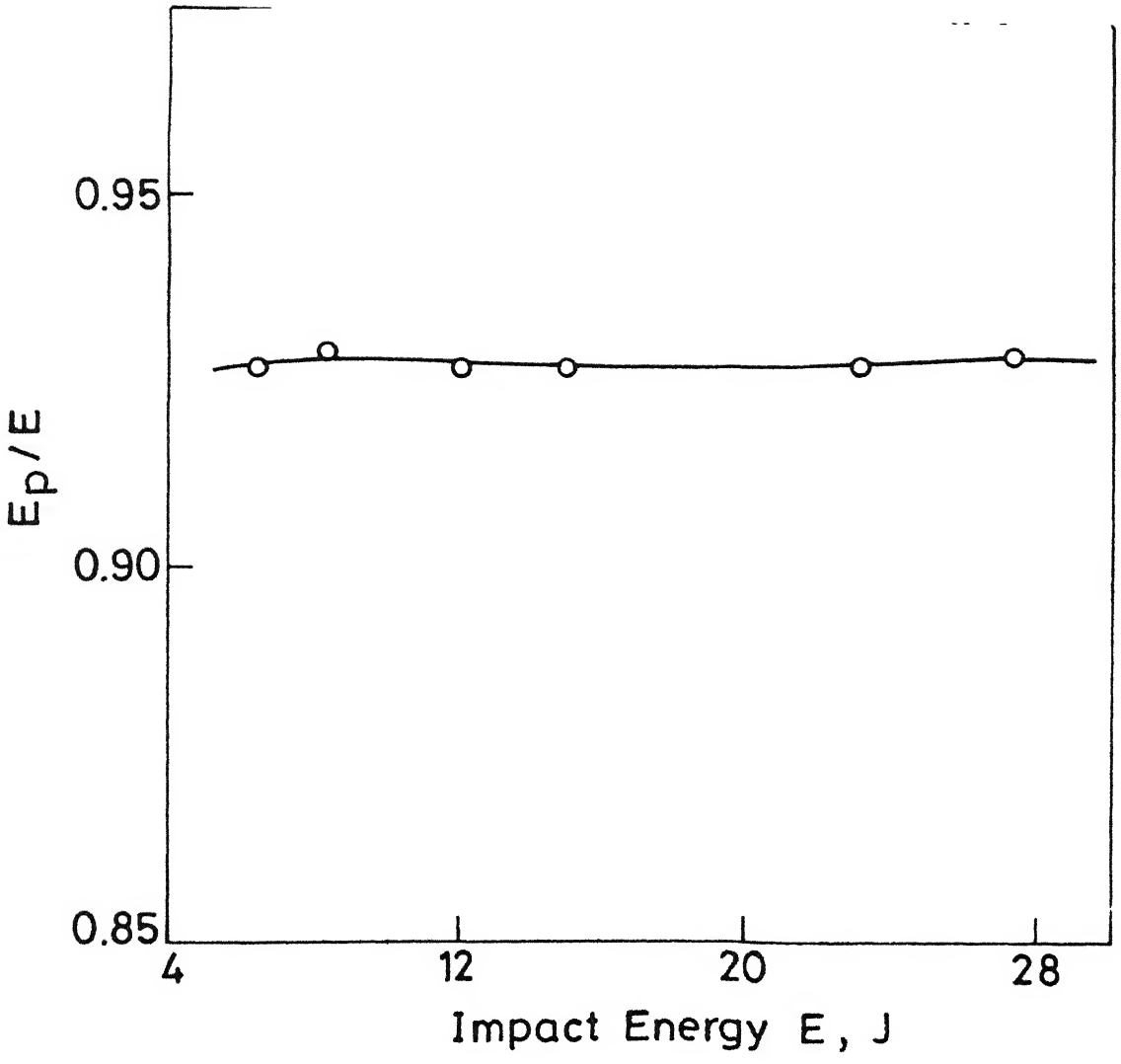

Fig. 5.15 Fraction of the total energy absorbed by the by the plate vs impact energy.

most of the energy (about 93%) of the impactor gets absorbed in the plate. Certain assumptions were made in the calculation of this energy. For using Eq. (4.2) in Sec. 4.6 for the calculation of plate velocity after impact, the contact period between the projectile and the panel should be so small that the plate does not rise much during this period. Since the pendulum (hanging plate) is quite long (1.27 m) and starts from rest, the initial motion of the plate is nearly horizontal. Thus only negligible error is expected in the calculation.

CHAPTER 6

CONCLUSIONS AND SCOPE FOR FUTURE WORK

The interlaminar fracture toughness values in mode I and mode II were found experimentally using energy release rate approach. The material used was glass fabric reinforced epoxy laminates. For mode I fracture toughness testing double cantilever beam (DCB) specimen was used. Various data reduction methods were examined and compared. For mode II fracture toughness testing,end notched flexure (ENF) specimen was used.

Out of the five DCB data reduction methods discussed, the compliance method which gave close values to that of nonlinear theory was chosen as the best method for finding G_{IC}. The G_{IC} obtained by this method was 699 J/m^2. Also, G_{IC} was found to be independent of crack length.

The mode II interlaminar fracture toughness G_{IIC} obtained was 1647 J/m^2. This value is found to be more than twice the value of G_{IC}.

Ballistic impact tests were conducted on clamped as well as hanging composite panels. The delamination area of the damaged plates were measured using a destructive technique. Results of fracture toughness tests were applied to the

impact problem to obtain the fraction of the impact energy dissipated in forming delamination cracks.

The damage on the impacted panels appeared to be independent of support conditions (clamped and hanging). Thus, the results of them were plotted together. The damage area increased with the projectile velocity nonlinearly. At 18 m/s of impact velocity,only barely visible damage was observed.

The damage on the rear side of the panel was found to be more than that on the impact side. Also four diagonal fracture planes along the fibre directions were identified on the impacted panels.

The fraction of energy absorbed in delamination showed an increase with increasing projectile energy. The energy absorbed in delamination was found to be 4-9% of the projectile energy. This is quite low and contradicts the notion that the delamination is a major energy dissipation mechanism in laminated composites. The hanging plate experiments showed that most of the energy (about 93%) of the impactor gets absorbed in the panel. This implies that about 4.5 to 10% of the energy absorbed in the plate is due to delamination.

Scope for Future Work

1. In the present work the fracture toughness obtained from the static tests were applied to the impact problem. To get more realistic solutions, finding the dynamic delamination fracture toughness will be useful.
2. G_I and G_{II} values can be correlated with impact resistance. For this purpose certain material factors such as type of fibre used or fibre volume fraction can be varied to get the above relationship. A residual compression strength can be found for the impacted panels to get a measure of delamination instead of the cut-strip method used in the present study.
3. The impact energy of the projectile gets dissipated in several ways. The different mechanisms of energy dissipation in the composite laminate can be studied.

APPENDIX A

DCB FIXTURE

Proper alignment of the hinges should be maintained for the loading of DCB specimens. A fixture was fabricated for the proper alignment and mounting of the hinges on the DCB specimen.

The fixture was made from 1" thick perpex glass sheet. A slot was made in the middle of it to insert the DCB specimen. Two adjustable screws at the bottom of the slot allowed position setting of the specimen, so as to have the proper alignments of the hinges with the specimen. The fixture with the DCB specimen is shown in Fig. A.1.

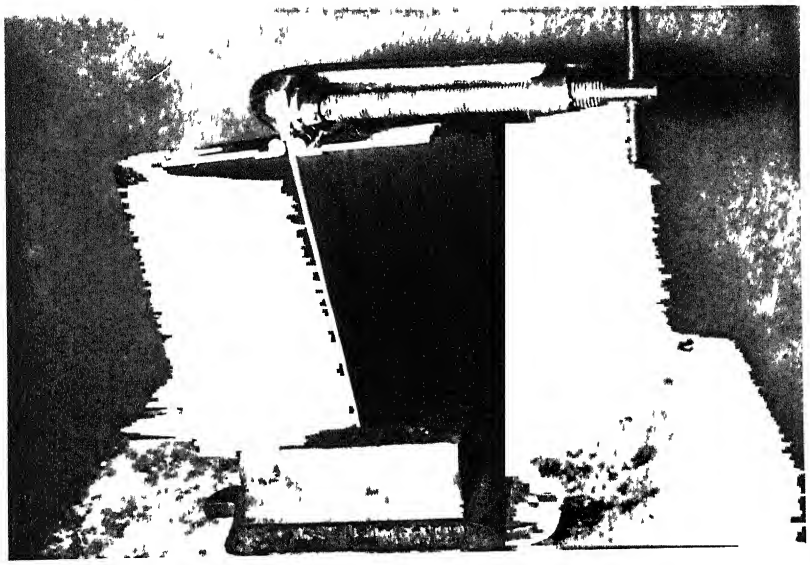

Fig. A1 DCB fixture with the specimen

APPENDIX B

EXPRESSION FOR STRAIN ENERGY RELEAS RATE G_{II}

The derivation for G_{II} is based on the change in compliance with crack extension. The compliance of the ENF specimen is defined as the displacement u at the central loading pin divided by the applied load, P. The expression for G_{II} can be obtained from the work of Carlsson et al. [14]. With the notations in Fig. B.1, u may be calculated as

$$u = \frac{\Delta_{AB} + \Delta_{BC} + \Delta_{CD}}{2} \qquad (B.1)$$

In the following derivation, deformation due to shear stress is neglected. The beams BC and CD are modelled as cantilever beams with elastic modulus E and thickness 2h. Assuming that the cross section at C does not warp because the line of load is an approximate line of symmetry, the following expressions can be calculated using Timoshenko [19] beam theory.

$$\Delta_{CD} = \frac{PL^3}{4Ewh^3} \qquad (B.2)$$

$$\Delta_{BC} = \frac{P(2L^3 + 3aL^2 + a^3)}{8Ewh^3} \qquad (B.3)$$

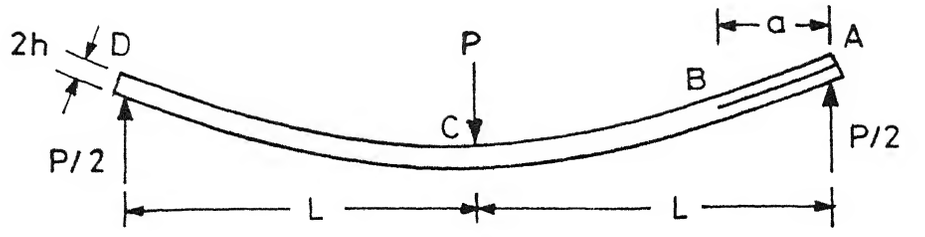

Fig. B1 ENF specimen in bending. Width of the specimen is w

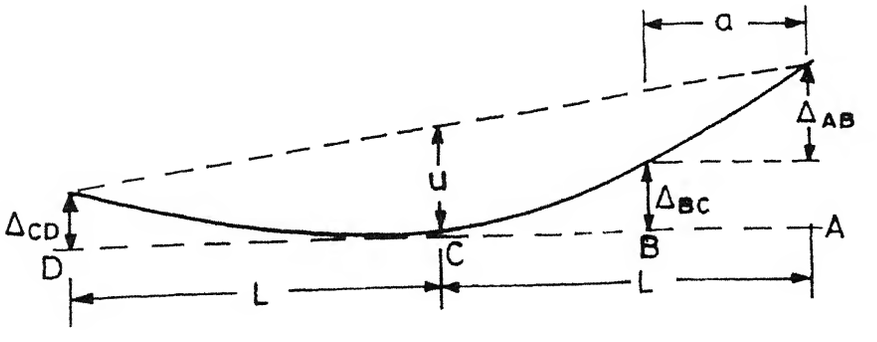

Fig. B2 Definition of vertical displacement for the ENF specimen.

For the delaminated region AB, the displacement Δ_{AB} has two components. One due to bending of the beams and other due to rotation of cross-section at Section B (Figs. B.1 and B.2). Assuming that each beam of the delaminated region carries the same load P/4, the displacement component due to bending may be calculated [19] from

$$\Delta_{AB,1} = \frac{Pa^3}{Ewh^3} \qquad (B.4)$$

The rotation of the cross-section at B is expressed as the slope of the cross section with respect to the horizontal axis. The slope of the cross section is obtained by summing up the slope produced due to a load P/2 and a moment M(= P/2 a) using expressions in [19]. The displacement component due to slope, $\Delta_{AB,2}$ is the slope at B multiplied by the length of the delaminated region. This gives

$$\Delta_{AB,2} = \frac{3P}{8Ewh^3}(aL^2 - a^3) \qquad (B.5)$$

Adding all the contributions to the displacement (eqns. B.2 - B.5) and substituting in eq. (B.1) gives the compliance as,

$$C = \frac{2L^3 + 3a^3}{8Ewh^3} \qquad (B.6)$$

Now using the general expression for energy release rate (eqn. 2.9) given in Sec. 2.3, that is,

$$G_{II} = \frac{P^2}{2w} \frac{dC}{da}$$

we get,

$$G_{II} = \frac{9a^2 P^2}{16Ew^2h^2} \qquad (B.7)$$

Since the compliance is experimentally evaluated, the modulus 'E' in Eq. (B.7) can be substituted in terms of compliance 'C' using Eq. (B.6) to get

$$G_{II} = \frac{9P^2Ca^2}{2w(2L^3+3a^3)} \qquad (B.8)$$

Eq. (B.8) was used in the evaluation of G_{II}.

APPENDIX C

ENERGY LOSS DUE TO AIR DRAG

In using the Eq. (4.2) in Sec. 4.6 the resistance due to the air is ignored. Since the moving object is a blunt flat plate energy loss due to air drag is expected. The correction to the velocity of plate after impact, is applied by finding the total drag losses, as explained below.

The drag force F_D on the plate is given by

$$F_D = \frac{C_D \rho V_r^2 A}{2}$$

where

C_D - coefficient of drag (for a square plate $C_D = 1.2$)

ρ - density of air ($= 1.2$ kg/m^3)

V_r - relative velocity of plate with air

A - area of plate

Relative velocity V_r varies from V_2 to zero. Hence, the total energy loss E_d due to drag is obtained by the integral of $F_D.ds$ along the path of the pendulum where ds is the incremental distance in the path. This was evaluated numerically using a computer programme in BASIC language attached at the end of

this appendix. The energy F_d.ds and the energy needed to raise the pendulum during that increment were subtracted from total energy of the plate, thus evaluating the kinetic energy of the pendulum at the end of increment ds.

Using the programme results, a curve is drawn between the corrected velocity and maximum height of the plate H (Fig. C.1). This curve which takes into account the drag energy loss was used to get the actual plate velocity after impact from the measured height H.

The curve of theoretical plate velocity (without considering air drag) is also drawn along with the corrected curve to have a comparison.

It can be seen from the figure that, the effect of wind drag is a maximum of 4% reduction in height of the plate and is negligible.

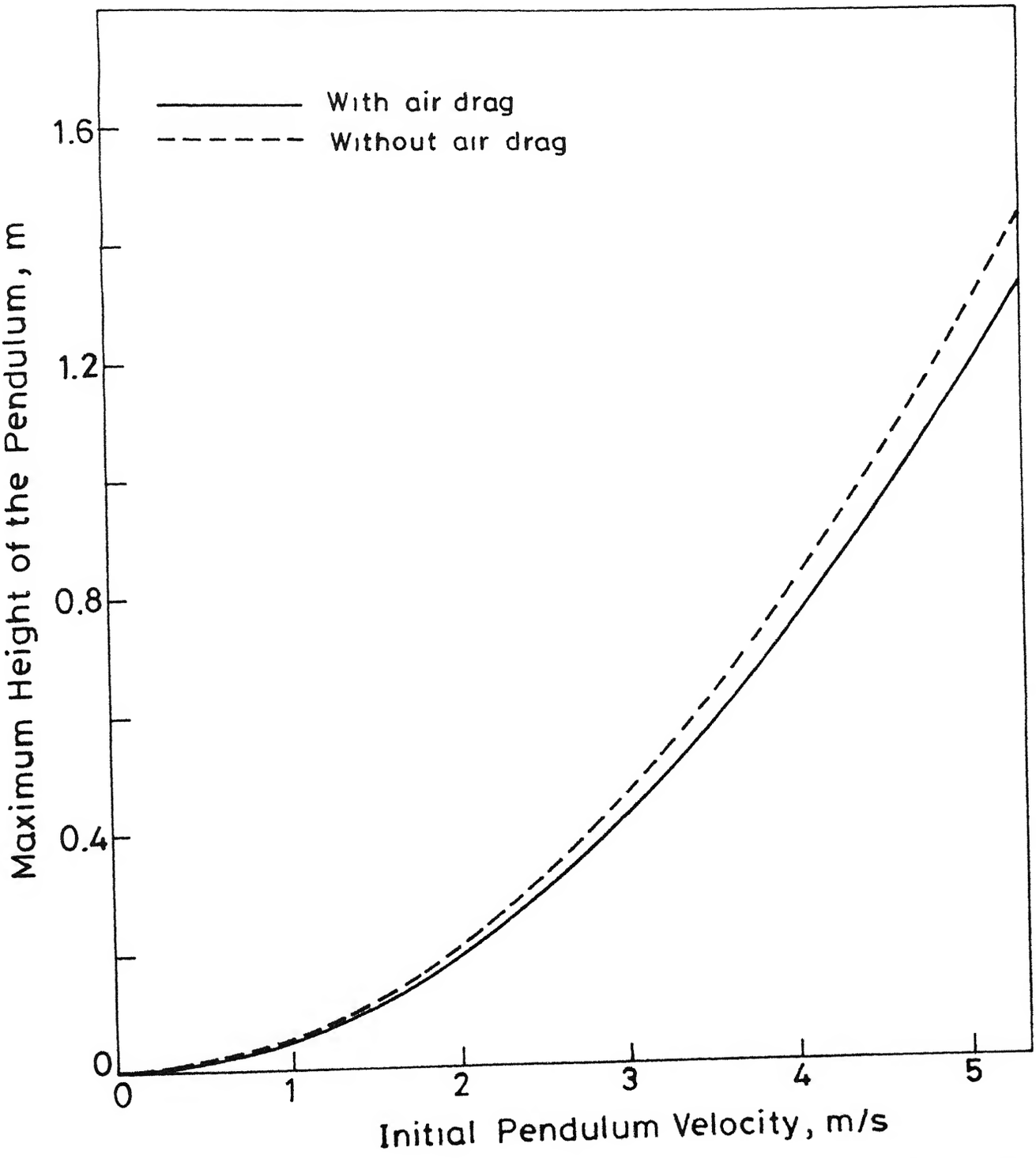

Fig. C1 Relations between maximum height of pendulum and initial pendulum velocity.

```
10 REM DRAG LOSS DUE TO AIR
20 READ R,L,B,M,D,CD
30 DATA 1 2762,  177, 177, 011[illegible]
40 V1= 5
50 FOR J=1 TO 6
60 V1=V1+1
70 I=1
80 K=0
90 REK=( 5*M*(V1 2)) T1
100 IF REK<0 THEN GOTO [illegible]
110 V2=SQR ((2*REK)/M)
120 H1=R*COS(TH)
130 TH=TH+ 00[illegible]8724
140 H2=R*COS(TH)
150 H=H1-H2
160 T3= 00[illegible]8724
170 D1=CD* 5*(V2 2)*R*L*B*T3*D
180 ED=ED+D1
190 G=M*9 809999*H
200 T=D1+G
210 IF K>0 THEN GOTO 390
220 T1=T1+T
230 I=I+1
240 GOTO 90
250 IF V2< 001 THEN GOTO 410
260 TH=TH- 00[illegible]8724
270 K=K+1
280 T2=T1-T
290 REK= 5*M*(V1^2)-T2
300 IF REK<0 THEN GOTO 410
310 K=K+1
320 V2=SQR((2*REK)/M)
330 H1=R*COS(TH)
340 TH=TH+ 0000[illegible]5
350 H2=R*COS(TH)
360 H=H1-H2
370 T3= 0000[illegible]5
380 GOTO 150
390 T2=T2+T
400 GOTO 290
410 H=R-H2
420 LPRINT J
430 LPRINT I,K
440 LPRINT V2,D1,C[illegible]
450 LPRINT T,REK,ED
460 LPRINT V1,H
470 NEXT
480 END
```

APPENDIX D

```
10  REM DCF DATA REDUCTION BY COMPLIANCE METHOD
20  DIM A(10),PC(10),DISP(10),FORCE(10),C(10),CL(10),DELTA(10)
30  DIM AL(10),PCL(10),SUMC(10),SUMA(10),SUMP(10),GICF(10)
40  L=0
50 ND=5
60  L=L+1
70 LPRINT L
80  READ N,W,M,F,H,CF
90  FOR I=1 TO N
100  READ A(I)
110  NEXT
120  FOR I=1 TO N
130  READ PC(I)
140  NEXT
150  FOR I=1 TO N
160  READ DISP(I),FORCE(I)
170  NEXT
180 FOR I=1 TO N
190 READ DELTA(I)
200 NEXT
210  REM COMPLIANCE OF EACH CURVE
220  FOR I=1 TO N
230  C(I)=(DISP(I)+M)/(FORCE(I)+ 4)
240  NEXT
250  REM CONSTANTS A1 AND A2
260  FOR J=1 TO N
270  CL(J)=LOG(C(J))
280  AL(J)=LOG(A(J))
290 K(J)=PC(J)+F+H
300  PCL(J)=LOG(F(J))
310  NEXT
320  SUMC(1)=CL(1)
330  SUMA(1)=AL(1)
340  SUMP(1)=PCL(1)
350  FOR I=2 TO N
360  K=I-1
370  SUMC(I)=CL(I)+SUMC(K)
380  SUMA(I)=AL(I)+SUMA(K)
390  SUMP(I)=PCL(I)+SUMP(K)
400  NEXT
410  ALA1=(SUMC(N)-N*SUMA(N))/N
420  ALA2=(SUMP(N)+SUMA(N))/N
430  A1=EXP(ALA1)
440  A2=EXP(ALA2)
450  REM CRITICAL ENERGY RELEASE RATE
460 GIC=3*A1*A2^2*(F+W)^2*1000
470 LPRINT GIC
480  REM ENERY RELEASE RATE USING EQUATION
490  FOR I=1 TO N
500 IJ= 5
510 IF L=1 THEN IJ=1
520  GICF(I)=3/2*DELTA(I)^2*M^2*(F+H)^2/(A(I)^2*W)^2*1000
530  LPRINT GICF(I)
540  NEXT
550  SUMG(1)=GICF(1)
560  FOR I=2 TO N
570  J=I-1
580  SUMG(I)=GICF(I)+SUMG(J)
590  NEXT
600  GICA=SUMG(N)/N
610  LPRINT GICA
```

```
620  GOTO 690
630  REM LOGA,LOGC AND LOGPC VALUE FOR 2 50mm
640  AC=50
650  CC=LOG(AC)
660  CA=ALA1+3*CC
670  PA=ALA2-CC
680  LPRINT CC,CA,PA
690 IF L<ND THEN GOTO 60
700 REM DATA DCB 1
710  DATA  5,25 4,1,1 0,1 0, 04
720  DATA 58 0,69 25,76 25,80 5 88 5
730  DATA 22 2,19 6,18 4,17 6 16 4
740  DATA 23 5,40 0,25 0,31 0, 0 0,25 5,28 0,23 5,30 0,19 0
750 DATA 30 5,38 5,47 5,53 5 64 5
760 REM DATA DCB 4
770 DATA 8,25 4,1, 5, 4, 01
780 DATA 38 0,43 8,52 0,57 6,64 ,71 0,76 3,85 5
790 DATA 166 0,162 ,137 ,116 5 108 ,100 ,85 5 82
800 DATA 11 ,57 5,15 ,61  21 ,61 , 21  45 ,48 ,71  49 ,62 5,50 5,50 ,70  52
810 DATA 30 ,37 5,48 ,60 ,73 ,87 ,98  121
820 REM DATA DCB 5
830 DATA 5,25 4,1  5, 4, 01
840 DATA 37 ,4  25 54 ,54 75 71 0
850 DATA 150 ,139 5 99  91 ,7
860 DATA 14 5,75 ,14 ,61  40 ,61  11 ,101  81 ,51 ,
870 DATA 28 5 44 ,65 ,9  ,130
880 REM DATA DCB 2
890  DATA 6,25 4 2, 5  4, 02
900   DATA 42 25,51 5 61 25,71  79 25,91 5
910  DATA 158  147  1 1 1 101 ,104 5
920  DATA 7 ,82 ,17 75,100 5,19 25,75 1,2  5,65 ,31 ,73 ,35 ,55 5
930  DATA 17 5,25 5,32 ,40 ,50 ,65
940  REM DATA DCB 3
950 DATA 7,25 4,1, 5, 4, 01
960  DATA 42 5,53 5,62 5,72 25,80 25,90 75,95 5
970  DATA 159 ,127 ,121 5,104 5 95 ,79 ,75 5
980 DATA 23 ,101 ,25 ,63 ,36 5,63 ,37 5,45 5,50 ,45 5,65 5,44 ,68 5,37 5
990  DATA 37 5,53 ,74 5,97 5,117  133 ,161 5
1000  END
```

REFERENCES

1. John E. Masters, 'Correlation of impact and delamination resistance in interleafed laminates', VI ICCM, vol. 3, 1987, pp 3.96-3.107.
2. B.D. Agarwal and L.J. Broutman, 'Analysis and performance of fibre composites', New York, John Wiley, 1980.
3. G. Morom, I. Roman, H. Harel and M. Rosensaft, 'The characterisation of Mode I and Mode II delamination failures in fabric-reinforced laminates', VI ICCM, vol. 3, 1987, pp 3.265-3.273.
4. W.D. Bascom, J.L. Bitner, R.J. Moultar and A.R. Siebert, 'The interlaminar fracture of organic-matrix woven reinforcement composites', Composites, January 1980.
5. L.J. Broutman and A. Rotem, 'Impact strength and toughness of fibre composite materials', Foreign object impact damage to composites, ASTM STP 568, 1975, pp 114-133.
6. Paul E. Keary and Larry B. Ilcewicz, Casey Shaar and Jess Trostle, 'Mode I interlaminar fracture toughness of Composites using slender double cantilevered beam specimens', J. of Composite Materials, vol. 19, March 1985, pp 154-177.
7. D.J. Wilkins, J.R. Eisenmann, R.A. Camin, W.S. Margolis and R.A. Benson, 'Characterising delamination growth in graphite epoxy', Damage in Composite Materials, ASTM STP 775, 1982, pp 168-183.

8. Kyung S. Han and James Koutsky, 'The interlaminar fracture energy of glass fibre reinforced polyster composites', J. Composite Materials, vol. 15, 1981, pp 371-388.

9. D.F. Devitt, R.A. Schapery and W.L. Bradley, 'A method for determining the mode I delamination fracture toughness of elastic and viscoelastic composite materials', J. Composite Materials, vol. 14, 1980, pp 270-285.

10. D. Guedra, D. Lang, J. Rouchon, C. Marais and P. Sigety, 'Fracture toughness in mode I: a comparison exercise of various test methods', VI ICCM, vol. 3, 1987, pp 3.347-3.357.

11. F.X. De Charentenay and M. Benzeggagh, 'Fracture mechanics of mode I delamination in composite materials', IV ICCM, 1980, pp 186-197.

12. S. Mall, G.E. Law and M. Katouzian, 'Loading rate effect on interlaminar fracture toughness of a thermoplastic composite', J. Composite Materials, vol. 21, 1987, pp 569-579.

13. A.J. Smiley and R.B. Pipes, 'Rate effects on mode I interlaminar fracture toughness in composite materials', J. Composite Materials, vol. 21, 1987, pp 670-687.

14. L.A. Carlsson, J.W. Gillespie, Jr., and R.B. Pipes, 'On the design and analysis of the end notched flexure (ENF) specimen for Mode II testing', J. Composite Material, vol. 20, 1986, pp 594-604.

15. Graham Dorey, 'Impact and crash worthiness of composite structures', Structural impact and crack worthiness, vol. 1, edited by G.A.O. Davies, July 1984, Elsevier Applied Science Publishers, pp 155-194.

16. R.L. Sierakowski and S.K. Chaturvedi, 'Impact loading in filamentary structural composites', Shock and Vibration Digest, vol. 15, No. 10, 1983, pp 13-31.

17. J.F. Liceaga and J.J. Imaz San Miguel, 'Impact behaviour of composite laminates', VI ICCM, vol.3, 1987, pp 3.108-3.122.

18. D. Lefebvre et C. Bathias, 'Delamination of composite materials. Fracture mechanics and damage evaluation', ICCM V 1985, pp 331-345.

19. S.P. Timoshenko and D.H. Young, 'Elements of strength of materials', East EWest Edition, 1968.

20. L.A. Carlsson and R.B. Pipes, 'Experimental characterization of advanced composite materials', Prentice-Hall Inc., New Jersey, 1987.

21. S. Hashemi, A.J. Kinloch and J.G. Williams, 'Interlaminar fracture of composite materials', VI ICCM, vol. 3, 1987, pp 3.254-3.264.

22. K.B. Su, 'Mechanisms of interlaminar fracture in a thermo-plastic matrix composite laminate', IV ICCM, 1985, pp 995-1006.

23. Joseph E. Grady and C.T. Sun, 'Dynamic delamination crack propagation in a graphite/epoxy laminate', ASTM, STP 907, 1986, pp 5-31.

24. N. Cristescu, L.E. Malvern and R.L. Sierakowski, 'Failure mechanisms in composite plates impacted by blunt-ended penetrators', Foreign Object Damage to Composites, ASTM STP 568, 1975, pp 159-172.

ME-1988-M-NAR-ENE